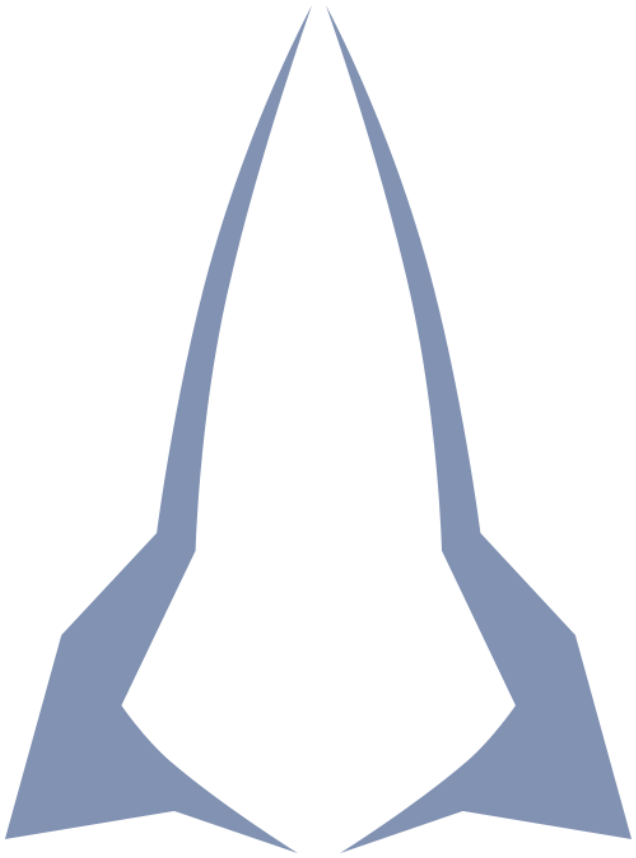

SPACEPORT TORONTO X VIENNA
PHASE 1 REPORT

UNIVERSITY OF TORONTO
VIENNA UNIVERSITY OF TECHNOLOGY (TU WIEN)

PROPULSION SUBSYSTEM PRELIMINARY DESIGN

Authors: Zeping Sun, Emerson Vargas, Jacob Weber, George Lu, Nguyen-cao, Mohamed Khalil

Driving Requirements

The following requirements are considered the main drivers of the propulsion subsystem.

1. Propulsion subsystem shall have a total impulse greater than 333,000 N·s and less than 899,600 N·s [*Base 11 System Requirements 3.1.16.2*].
2. System shall reach an apogee between 100 km and 150 km above ground level [*Base 11 System Requirements 3.1.16.1*].
3. The propulsion system shall be bipropellant liquid-fueled [*Base 11 System Requirements 3.2.4.1*].

Subsystem Block Diagram (SSBD)

The SSBD details the interactions happening within the subsystem, and between a subsystem and the others.

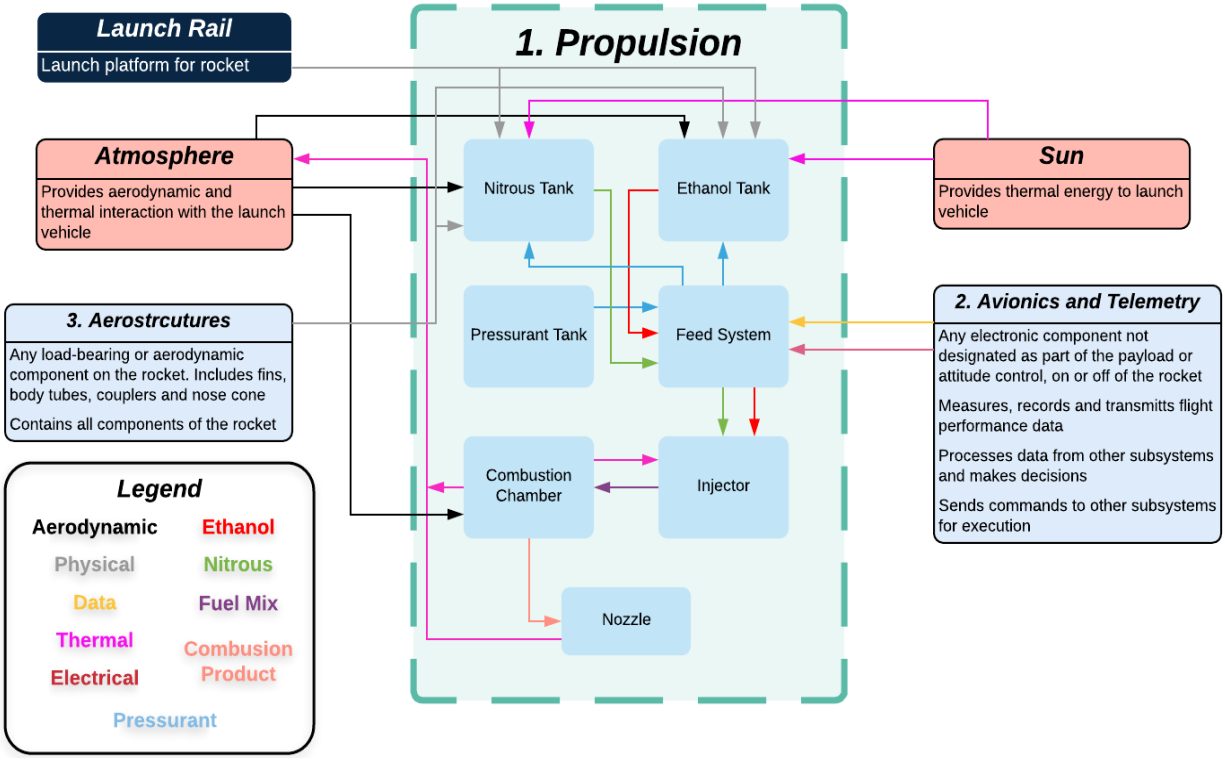

Figure 15 - Propulsion SSBD

Table 26 - Propulsion Subsystem Interface Descriptions

Interface ID	Parent	Child	Direction	Purpose
Thermal_Ext_01	Sun	Ethanol Tank	One way	Provides thermal energy to the ethanol tank
Thermal_Ext_02	Sun	Nitrous Tank	One way	Provides thermal energy to the nitrous tank

Data_Ext_01	Avionics	Feed System	One way	Senses the pressure of the operating fluids
Electrical_Ext_02	Avionics	Feed System	One way	Sends the signal to actuate fluid flow
Physical_Ext_01	Launch Rail	Ethanol Tank	One way	1/2 launch lug will be attached to the bottom of the ethanol tank
Physical_Ext_02	Launch Rail	Nitrous Tank	One way	2/2 launch lug will be attached to the bottom of the ethanol tank
Aerodynamic_Ext_01	Atmosphere	Ethanol Tank	One way	The ethanol tank is also the airframe of the rocket for that portion of length and therefore, exposed to the atmosphere
Aerodynamic_Ext_02	Atmosphere	Combustion Chamber	One way	The combustion chamber was designed to be exposed to air to greater utilize convective cooling
Aerodynamic_Ext_03	Atmosphere	Nitrous Tank	One way	The nitrous tank is also the airframe of the rocket for that portion of length and therefore, exposed to the atmosphere
Physical_Ext_03	Aerostructures	Ethanol Tank	One way	Ethanol tank end caps will be bolted to the composite body tubes to make up the airframe
Physical_Ext_04	Aerostructures	Nitrous Tank	One way	Nitrous tank end caps will be bolted to the composite body tubes to make up the airframe
Ethanol_Int_01	Ethanol Tank	Feed System	One way	Provides an ethanol source for the feed system
Nitrous_Int_01	Nitrous Tank	Feed System	One way	Provides a nitrous source for the feed system
Pressurant_Int_01	Feed System	Ethanol Tank	One way	Provides a pressurant source for the ethanol tank
Pressurant_Int_02	Feed System	Nitrous Tank	One way	Provides a pressurant source for the nitrous tank
Pressurant_Int_03	Pressurant Tank	Feed System	One way	Provides a pressurant source for the feed system
Ethanol_Int_02	Feed System	Injector	One way	Provides ethanol to the injector
Nitrous_Int_02	Feed System	Injector	One way	Provides nitrous to the injector
Fuelmix_Int_01	Injector	Combustion Chamber	One way	Injects both nitrous and ethanol into the combustion chamber for mixing, atomization, and combustion
Thermal_Int_03	Combustion Chamber	Injector	One way	High heat transfer from combustion chamber to injector
Thermal_Int_04	Combustion Chamber	Atmosphere	One way	Combustion chamber transfers heat to the atmosphere through both radiation and convective modes
CombustionProduct_Int_01	Combustion Chamber	Nozzle	One way	Combustion products are ejected out of the combustion chamber and into the nozzle

Thermal_Ext_05	Nozzle	Atmosphere	One way	Nozzle transfers heat to the atmosphere through both radiation and convective modes

Physical Architecture

Propellant Feed System

PEAK Technology

The propellant tanks and most probably the nitrogen pressurant tanks will be manufactured and tested by our sponsor - “PEAK Technology”. Peak Technology is a high-tech company in Austria that specializes in lightweight structures and composite solutions. They have been a very important sponsor to TUST for several years and helped designing and manufacturing the airframe and components of different sounding rockets.

They will also work together with TUST and UTAT in the Base11 Space Challenge and design the pressure tanks and other components in close cooperation. They have the experience and know-how to design, build and test composite pressure vessels. PEAK Technology is very interested to make a project succeed, so they can demonstrate their capabilities in the aerospace section and receive some flight proven hardware. By this reason, we can count on their support where it is possible for them e.g. parts of the plumbing system and the composite aerostructure. A cold static pressure test with some thrust chamber material at their facility has already been performed.

Trade Studies

The purpose for trade studies is to systematically determine the optimal design choice for the rocket. To start off, the Philosophy and Functional Evaluations are conducted in each trade study to determine the team’s priorities with this design. Following, these priorities are treated as metrics to evaluate the multiple choices in a multi-stage Pugh decision matrix with a favorable “+” or unfavorable “-” position. The qualitative Functional Evaluation results are used to support the team’s reasoning in position assignment for each candidate solution considering the Philosophy Criteria shown in the second table. Lastly, more detailed explanations behind the “+” and “-” assignments are provided afterwards in the third table.

Tank Configuration

This trade explores the various possible arrangements of the propellant and pressurant tanks in the system. The tandem configuration uses separate pressurant tanks for the fuel and oxidizer and places these tanks nearest to the corresponding fluid. In a coaxial configuration, the fuel tank is contained inside of the oxidizer tank or vice versa with only one set of pressurant tanks required. An in-line arrangement also uses only one set of pressurant tanks but requires plumbing to pass the pressurant lines through one of the propellant tanks into the other beneath it. This trade study includes the effects of the team’s partnership with PEAK Technologies. Note that due to the results in the first comparison table below, the coaxial and floating configurations were not considered for further development.

Table 27 - Philosophy Criteria Evaluation

Criteria	Safety	Simplicity	Cost	Reliability	Performance	Robustness	Score
Safety		1	1	1	1	1	5
Simplicity	0		1	0	1	1	3
Cost	0	0		0	1	1	2
Reliability	0	1	1		1	1	4
Performance	0	0	0	0		1	1

Robustness	0	0	0	0	0		0

Table 28 - Functional Evaluation

Configuration	Tandem	Coaxial	In-line	Floating
Pressurant Tanks	2	1	1	2
Propellant Tanks	2	1	2	2
Manufacturability	Simple	Impossible	Complex	Complex
Mass	Heavy	Light	Heavy	Light
Centre of Gravity	Lower (Worse)	Middle	Higher (Better)	Variable (gets worse)
Number of Plumbing Parts	Greatest	Low	Middle	High
Pressure Coupling	None	Propellant & pressurant	Pressurant	None
Operational Complexity	High	Medium	Low	High
Control Complexity	Low	High	Medium	Low
Assembly Misalignment Tolerance	High	High	Low	Low
Cost	Low	High	Medium	High
Cleaning/Maintenance Complexity	Low	High	Low	Medium
Material Compatibility Issues	None	Some (inner tank exterior)	None	More (floating tanks exterior & electrical)
Actuator & Instrumentation Accessibility	High	Medium	High	Low

Table 29 - Candidate Evaluation

Criteria	Weight	Tandem	Coaxial	In-Line	Floating
Safety	0.33	+	-	+	-
Simplicity	0.20	+	-	+	-
Cost	0.13	+	-	+	-
Reliability	0.27	+	-	+	-
Performance	0.07	-	+	+	+
Robustness	0	+	-	+	-
Total:		0.93	0.07	1.00	0.07

Table 30 - Candidate Evaluation

Criteria	Weight	Tandem	In-Line
Safety	0.33	+	-
Simplicity	0.20	+	-
Cost	0.13	+	-
Reliability	0.27	-	+
Performance	0.07	-	+
Robustness	0	=	=
Total:		0.66	0.34

Based on the information presented above, the tandem tank configuration was selected. The tandem tank configuration offers superior safety over all the other configurations, owing to the independent operations of the propellant and pressurant tank pairs for the fuel and oxidizer. This increased safety, along with the resulting simpler controls, maintenance and increased assembly tolerances all offset the increase operational complexity that stems from the increased number of plumbing components. The tandem configuration simplifies the control of the propellant feed system because the pressures in the oxidizer and fuel tanks can be controlled independently from their respective pressurant tanks. The increased number of components in the tandem configuration compared to the in-line configuration does result in a lower centre of gravity and increased mass over the in-line configuration. Each of the configurations examined are sufficiently robust as they can all operate in the environments and climates typical to Vienna, Toronto and Spaceport America.

Tank Type

There are five types of composite tanks.

- Type I: All-metal construction.
- Type II: Thinner metal construction, with a fiber-reinforced polymer overwrap in the hoop direction. The metal vessel and wound composite materials share structural loading.
- Type III: Metal liner with full carbon fiber composite overwrap.
- Type IV: Polymer liner with full carbon fiber composite overwrap.
- Type V: A liner-less construction, with an all-composite vessel.

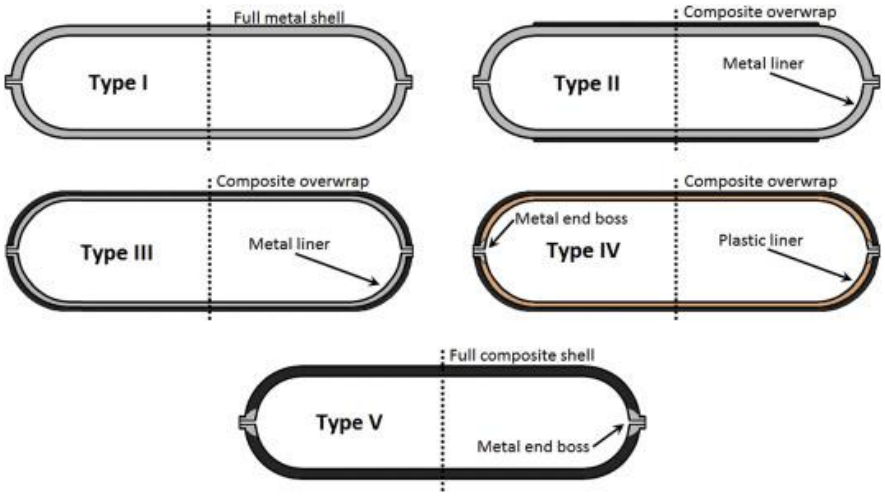

Figure 16 - Types of Composite Tanks [12]

This trade explores the various designs of qualified propellant tanks for the system. The purpose for this study is to systematically determine the optimal tank for our rocket. The weighting for the design values is identical to that employed for the Tank Configuration trade study and is not duplicated here for conciseness (refer to Table 27).

Table 31 - Tank Type Functional Evaluation

Type	I	II	III	IV	V
Mass	Highest	High	Medium	Low	Lowest
Permeability	None	None	None/low	None/Low	Low
Manufacturability	Simple	Simple	Middle	Middle	Complex

Design Process	Simple	Simple	Middle	Complex	Complex
Professional Support	None	None	None	High	None
Cost	Medium	Medium	High	High	High
Sponsoring	None	None	None	High	None

Table 32 - Tank Type Candidate Evaluation

Criteria	Weight	Type I	Type II	Type III	Type IV	Type V
Safety (professional manufacturing)	0.33	+/-	+/-	+/-	+	+/-
Simplicity	0.20	+	+	+	-	-
Cost (including sponsoring)	0.13	-	-	-	+	-
Reliability	0.27	+	+	+	+	+
Performance	0.07	-	-	+	+	+
Robustness	0	+	-	-	-	-
Total:		0.635	0.635	0.705	0.8	0.505

PEAK Technology is interested in experimenting with Class 4 tanks, and thus, they are very eager to support the team with designing and constructing this type of tank for the competition. The decision was made to proceed with a Type IV tank.

Propellant Delivery Method

In any liquid or hybrid rocket, propellants are stored separately and must be fed into the thrust chamber, mixed and burned to generate thrust. There are two common methods for driving the propellants out of their tanks and into the thrust chamber: pressure-fed and pump-fed. A pressure-fed system stores the propellants at high pressures and simply uses this pressure head to force the fluids through the plumbing and into thrust chamber. The pressure is limited by mass requirements but constrained by the required mass flow rate across the injector. A pump-fed system bypasses the limitation of the tank pressure by including turbopumps to move the propellants. Once again, refer to Table 27 for design value weighting.

Table 33 - Propellant Delivery Method Functional Evaluation

Method	Pressure	Pump
Propellant Tank Mass	Heavier; designed by internal pressure	Lighter; designed by ground and flight loads
Additional Components	Pressurant tanks	Pumps
Mass of Additional Components	Lower	Higher
Overall Simplicity	Simpler	More complex
Range of Possible Flow Rates	Very constrained	Flexible
Sensitivity to Ambient Conditions	High	Low
Controllability of Flow Rates	Low	High

Table 34 - Propellant Delivery Method Candidate Evaluation

Criteria	Weight	Pressure-Fed	Pump-Fed
Safety	0.33	+	-
Simplicity	0.20	+	-
Cost	0.13	+	-

Reliability	0.27	+	-
Performance	0.07	-	+
Robustness	0	-	+
Total:		0.93	0.07

The pressure-fed system requires less plumbing and no pumps but more pressurant tanks and actuators. A major part of this trade off study is linked to the trade-off of the units of components needed for each candidate. The pressure-fed system scored higher on safety because it was able to decouple the pressurant tanks and it didn't require a pump. There are numerous rocket failures due to pumps due to its design, manufacturing, and debris contamination. The team would require high quality pumps to not only ensure performance, but also safety. Given that the team's also working on a limited budget, it's unlikely the team can find an N_2O-safe pump that can also perform under potential 2-phase flow characteristic. Pump-fed systems also require the addition of new power source into the system. Regardless of whether this power system is electrical or thermal in nature, the expected complexity far exceeds that of a pressure-fed system.

While a pump-fed system is superior in performance because it allows a greater range of possible flow rates, greater control of flow rates, and is less sensitive to ambient conditions such as temperature, it's also less reliable as the team does not have the experience required to operate and maintain the machinery. On the other hand, the team has some experience in self-pressurizing fluids (N_2O) and hybrid rockets. The combination of both is transferable to implementing a pressurization system. This system in general not only requires less components, but less expensive components in general. The pressurant tanks will be fully sponsored by the team's sponsor PEAK. Lastly, the pressure-fed candidate was deemed superior in simplicity and cost as it required fewer plumbing components in general and did not need the volume envelope to support a pump. In summary, the team will proceed with the pressure-fed system.

Design Proposal

Through the Tank Configuration trade study, four designs were initially narrowed down to a final two. Then the two final designs were evaluated in a true pair-wise comparison manner to determine the optimum design. Simultaneously, five unique tank types were also evaluated. It was discovered that the tandem configuration and pressure-fed designs in combination with the Type IV tanks were superior to alternatives and will be utilized in the proposed design.

The propellant feed system covers all of the thermo-fluid high-level system architecture of the propulsion system. For electrical control of actuators and sensors, refer to Avionics Subsystem Preliminary Design. In this system, the two main system-level uncertainties were the tank configuration and the propellant feed method. After collective brainstorming sessions, the team arrived at four potential tank configurations and two potential feed methods. In order to narrow both down to a single design each, a trade study was conducted on each decision to ascertain the optimal design. The following diagrams present the fill and flight feed system schematics and physical architecture.

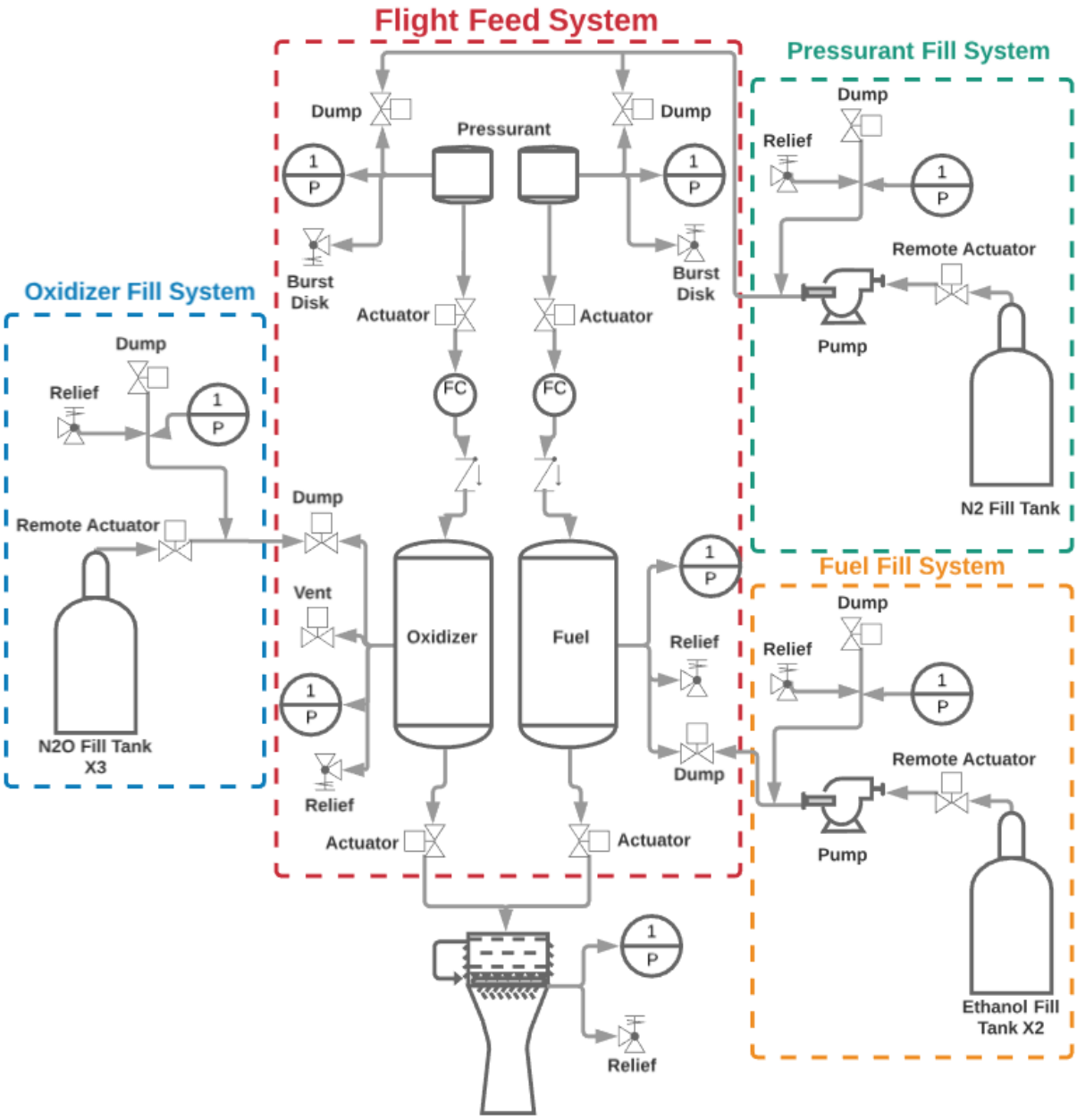

Figure 17 - Flight and Fill System P&ID

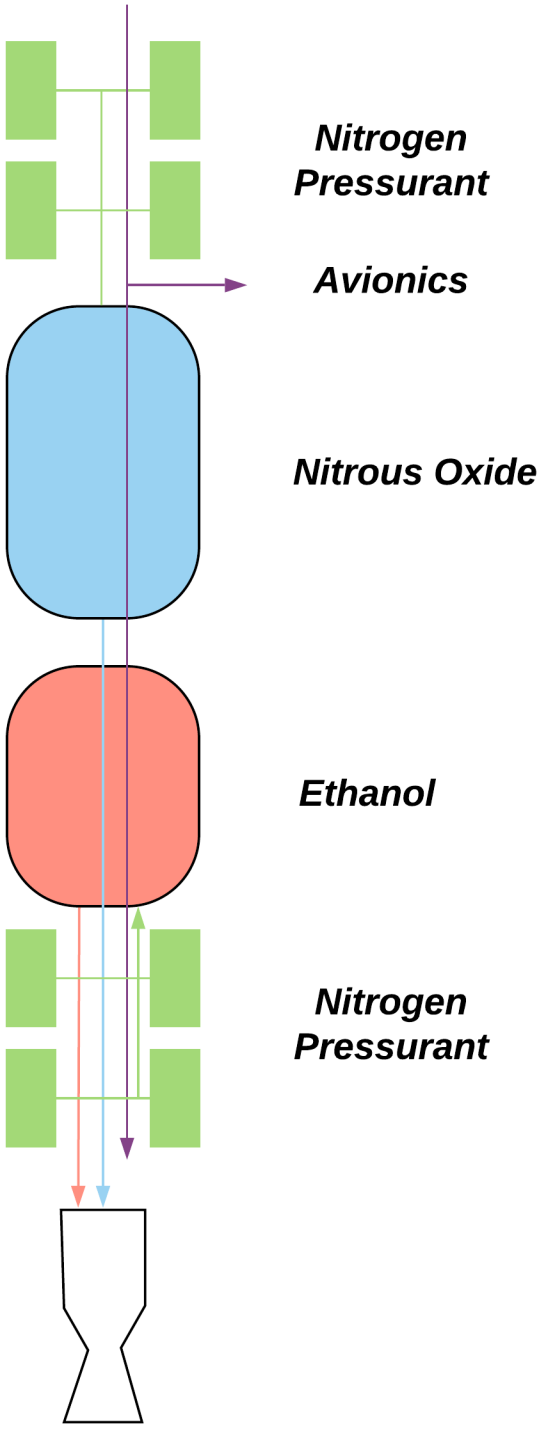

Figure 18 - Physical Architecture Diagram (valves excluded)

Propellant Fill Systems

While both systems fill different fluids, the plumbing requirements are almost standard between them. A remote actuator will be placed following after the K-Type outlet in order to allow the team to fill remotely. In order to fill the oxidizer from the fill tank, its flight tank will include a vent in order to maintain an ullage of gas to allow further liquid draw from the fill tank [13]. The team will likely pre-fill the oxidizer tank with nitrogen prior to the nitrous oxide to minimize nitrous oxide loss due to venting. No pump will be used for the oxidizer fill process. On the other hand, the fuel filling process will be identical to the oxidizer except that instead of a filling by venting, a pump will be used instead because ethanol will remain liquid within the operating conditions.

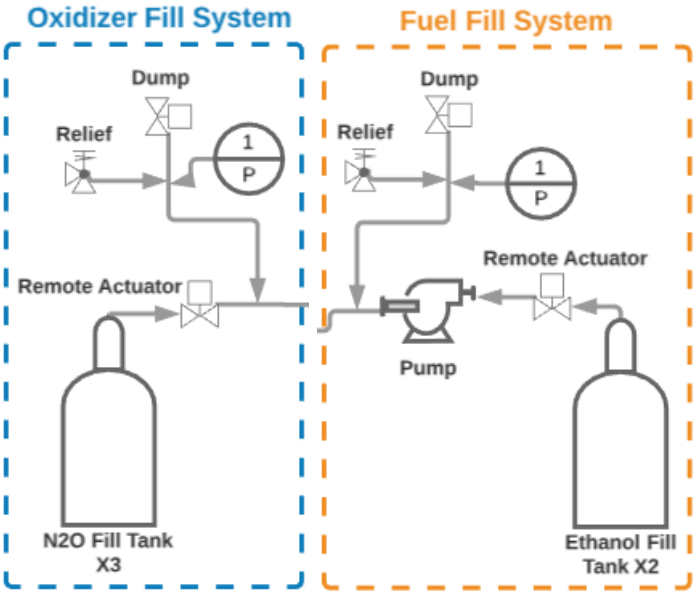

As per Base 11 Safety Training, a relief and dump valve sub-unit is attached to any section of the plumbing that can trap pressure. A pressure transducer is added to the fill lines in order to inform the team of when it is safe to remotely disconnect the umbilical from the rocket during the launch sequence. That said, the details of umbilical separation have yet to be determined. The team has successfully operated with a nylon tubing and remote cutter in the past to disconnect umbilicals. However, this was performed on 0.25-inch plumbing. Whether or not the team will decide to proceed with a similar diameter fill line is in future works.

Pressurant Fill System

The configuration depicted enables filling of the pressurant tanks when the rocket is mounted on the rail. It is also possible for the tanks to be filled prior to assembly, by the manufacturer and the team's sponsor, PEAK Technology. The tanks are rated and certified for human use [14] and thus satisfy Base 11 System Requirement 3.2.4.14 regarding the necessary safety factor for safe handling of pressurized vessels. The main advantages of the pre-filling approach are the reduced system mass, since none of the components necessary for filling need to be included on the rocket and the increased simplicity during assembly. In addition, the filling procedure for the nitrogen pressurant would be very difficult to accomplish in the environment at the launch site as it requires pressurizing nitrogen to 4,500 psi and in supercritical conditions.

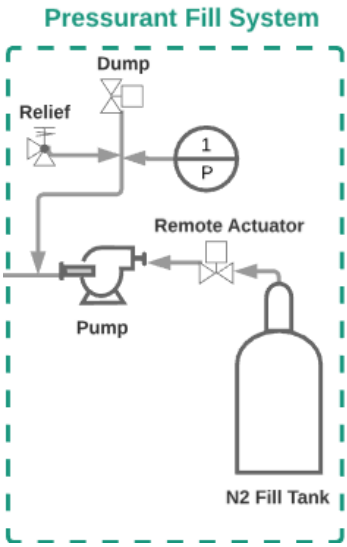

Flight Feed System

The trade studies conducted on the tank configurations and propellant feed methods led to the team's decisions to proceed with a tandem tank and pressure-fed system. The blowdown model allowed the team to provide a reasonable estimate of the mass flow rate over time needed for both the propellants and the pressurant to reach the necessary engine performance. Through iterating between design and analysis, the team narrowed down critical thermophysical properties (pressure, mass flow rate, mass, density) of the fluids involved and was able to estimate the diameter of the plumbing lines needed. The flow velocity and head loss were estimated using Bernoulli's Principle and the Colebrook equation as per Crane TP-410 [15]. If the N_2O lines will be pre-chilled prior to operation and the pressure from the pressurant is high enough, the team can assume the N_2O will

flow in a liquid state. Results from preliminary estimates are shown in the table below. The following assumptions were made for the calculations:

1. Thermal equilibrium
2. Steady state flow
3. Incompressible

Table 35 - Preliminary Plumbing Sizing

	Oxidizer	Fuel	Pressurant to Oxidizer	Pressurant to Fuel
Pressure (bar)	36 (522 psi)	35 (508 psi)	300 (4,531 psi)	300 (4,531 psi)
Mass flow rate (kg/s)	2.07	0.863	0.108	0.0414
Mass (kg)	126 (278 lbs)	52.5 (116 lbs)	2.3	2.88
Phase	Liquid	Liquid	Supercritical	Supercritical
Temperature (K)	278	293	278	278
Density (kg/m^3)	882	789	300	300
Stored Volume (m^3)	0.143	0.0665	0.00767	0.0096
Hydraulic Diameter (mm)	7.58	9.60	< 1	< 1
Pipe Diameter (inch)*	0.5”	0.5”	0.25”	0.25”
Friction Loss (Pa/m)	2.9E-10	3.1E-10	8.2E-12	7.9E-12
Re	8E+06	5E+05	3E+07	3E+07
D’Arcy Friction Factor, f_D	0.027576748	0.028418	0.034021599	0.034021547
Tank Length (mm)	2,389	1,196	-**	-**

*North American standard unit for plumbing.

**These tanks will be standard sizes, so length was not a computed parameter.

Propellant Tanks

The tanks are structural components that serve purposes in both the propulsion and aerostructures subsystems. This design, given the selected tank materials and type, enables a lighter rocket, because there is no need for an additional airframe tube. Type IV tanks use a plastic liner in which the propellant is stored. A full carbon fiber composite overwrap carries the structural loads. These tanks require a complex bulkhead, which is a machined aluminium part, and is bonded in between the plastic and the composite structure. The tanks are designed and manufactured in close cooperation with our sponsor PEAK Technology.

Currently, the nitrous oxide tank will be positioned above the ethanol tank, as this minimizes the amount of propellant bypass tubing, as well as provides a slightly higher centre of gravity location. The tanks are independent vessels, and will be mechanically connected with a coupler, most likely constructed out of solid carbon fiber composite. This coupler will be designed in close cooperation with PEAK Technology, as their experience with the Airbus Zephyr project provides with ample experience with composite couplers.

Since the tanks are structural airframe components, it is not possible to lay any wiring or piping on the outside of the tanks without proper containment (fairings, high temperature tape, etc.). At this stage, it is desirable to avoid external wiring and plumbing lines, since the exact aerodynamic conditions (especially heating) are unknown or knows to a lesser extent than the tank internal conditions. This means that currently, it is necessary to route certain plumbing and the datacom lines through the tanks. At least one nitrous oxide pipe must pass through the ethanol tank and one electrical data cable through both tanks. The sealings of the pipes must be executed like there are no unexpected structural loads because of lengthening in consequence of pressuring the tanks. This will be ensured by seals that are which are flexible in axial direction on one side of the bypass tubes. The ethanol will be pressurized from a nitrogen tank below through a rising pipe and the nitrous oxide will be pressurized from above without a rising pipe.

For both tanks there is monitoring for pressure and for temperature and a pressure relief burst disc on each tank to make sure critical pressure is never reached. It will be necessary to cool down the tanks when they are filled, especially the nitrous oxide tank is very temperature sensitive and should never reach critical pressure. This cooling process is very easy to achieve simply by letting the nitrous tank continuously vent to atmosphere. Even in temperatures as high as 48°C, such as at Spaceport America, UTAT has managed to chill the nitrous tank via this approach. Insulative approaches will also be investigated to control the nitrous temperature after disconnecting the fill system and closing the vent.

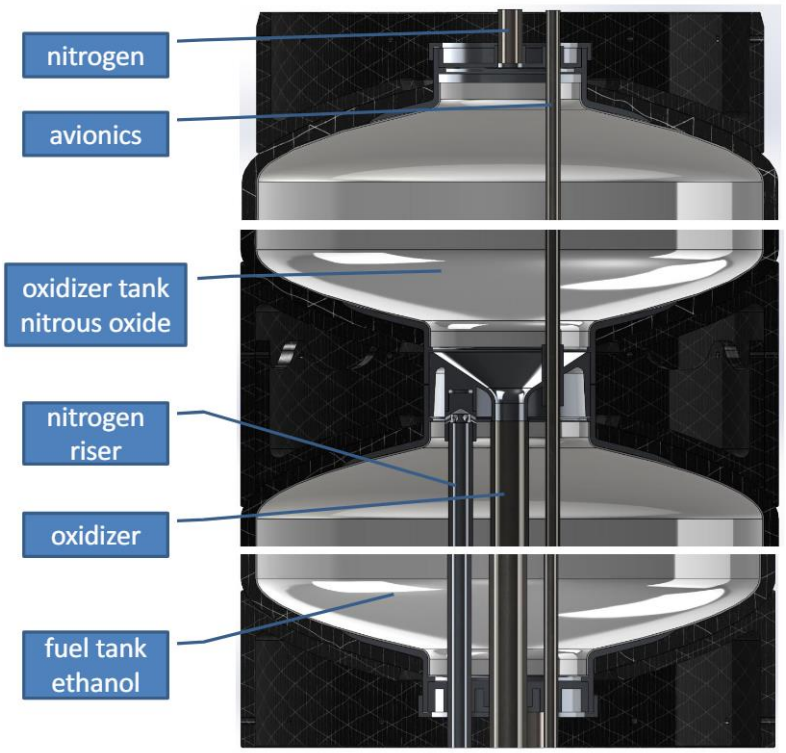

Figure 19 - Tank Bulkhead and Bypass tube design

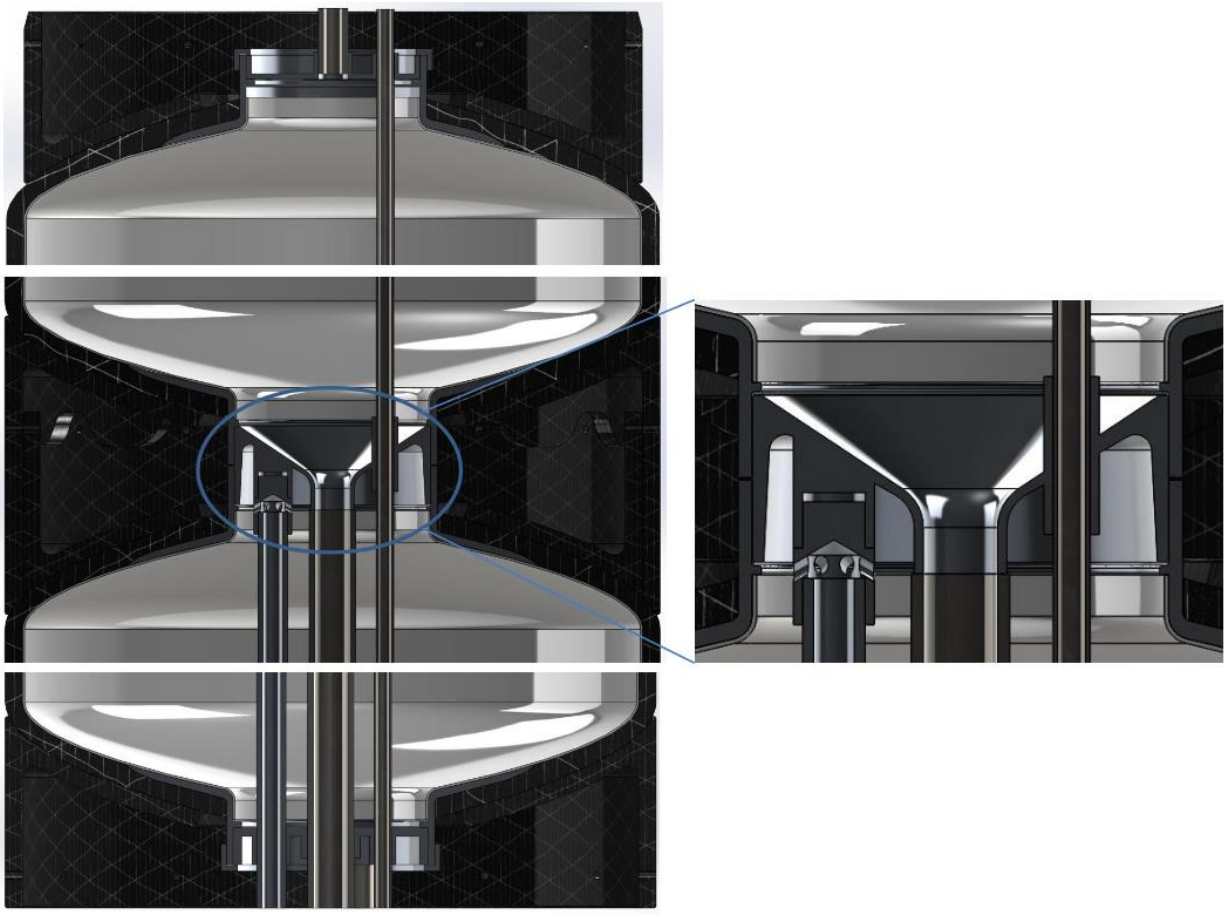

Figure 20 - Nitrous tank lower bulkhead, showing nitrogen rising tube for ethanol and the avionics datacom bypass tube

The total length for both propellant tanks is 3.585 m measured from the top nitrous tank bulkhead to the bottom ethanol tank bulkhead. The actual design of the bulkheads considers that there has to be some margin in size, in case some pipe cross sections have to be larger in the final design.

Baffles

To reduce the movement of a free fluid surface ('sloshing') on the dynamic behavior of the tank, it is necessary to install baffles into the propellent tanks. This is especially critical for fluids like nitrous oxide, whereby a large surface area to volume is required to quench any possible localized spontaneous decomposition (an effect of adding baffles). At this time, the calculations for the baffle design haven't started yet, because this will be done in close cooperation with our sponsor PEAK Technology during the detailed design phase. The proposed design is the honeycomb structure, which is mostly used for purposes like this. The width of the polygons should be as small as necessary but as big as possible, so the infill is as light as possible to fulfill its function.

Avionics Cable Duct

It is necessary to connect the upper and the lower avionics by electric wiring. For this reason, a cable duct with 6-7 mm internal diameter will be installed. This pipe will pass through both propellant tanks like shown in the figures above. To prevent any static charge relative to the tank walls from building up on the duct, the duct will be made out of (slightly) conductive material like carbon fibre or metal and will be electrically connected to the tank.

Preliminary Analysis

In order to model the performance of the propellant feed system, and thus the whole propulsion subsystem, a few things must be achieved in order to guarantee the analysis will produce results that are representative of the real system. Those main things are:

Table 36 - Required models for analysis

Item	Description
Nitrous Oxide blowdown model	A model that can predict the simple pressure blowdown physics of nitrous oxide. The model must produce mass flow rate, tank pressure and temperature data as its outputs, as well as the required tank volume based on initial conditions (initial temperature and mass)
Pressurization model	A model that can predict the physics associated with pressurizing a tank of nitrous oxide with an inert gas.
Nitrous oxide thermophysical properties	A model for pressure and density based on temperature for nitrous oxide
Combustion chemistry model	A model that can predict equilibrium combustion chemistry in the combustion chamber

Nitrous Oxide Blowdown Model

This model is designed based on a master's thesis by Margaret Mary Fernandez [16] which was concerned with the problem of nitrous oxide blowdown. The model consists of two control volumes, one being the liquid nitrous, and one being the vapour phase on top of the liquid phase. The model assumes quasi-static thermal equilibrium between the liquid and vapour phases, and achieves that by evaporating a small portion of the liquid phase into the vapour phase. This increases the number of moles present in the vapour phase (ullage), and thus, increases the pressure. This is true to nitrous oxide's self pressurizing capability. The thermodynamic imbalance between the phases is driving by the loss of liquid nitrous due to blowdown, which is modelled using pressure differential between the tank and injector head (chamber side) pressure, plumbing pressure drop, injection orifice side and a discharge coefficient.

The model assumes the following:

Table 37 - Blowdown Model Assumptions

Assumption
The tank drains such that the temperature, T, and the pressure, P, of the liquid and gas phases are uniform for all instants in time throughout the draining process; thus, the tank contents are always in phase equilibrium.
The gravitational head in tank (hydrostatic force) is negligible.
Tank walls are adiabatic.
Tank walls are always in thermal equilibrium with the tank contents.
The potential and kinetic energy of liquid and gas phases are negligible.
The Ideal Gas Law supplies Pressure, Temperature and volume closures
Pressurant gas is non-condensable and resides totally in the gas phase (non-soluble in oxidizer)
Pressurant gas is inert
Pressure drop between the oxidizer tank and the combustion chamber drives flow, and these effects are incorporated via a discharge coefficient. Frictional losses are neglected in the tank.
Pressurant addition is a quasi-static process.

Evaporation occurs at the interface between the liquid and gas phases. Due to the equilibrium nature of the models, no boiling occurs in the tank.

The following diagram illustrates the physical setup of the system and the control volumes used for the analysis:

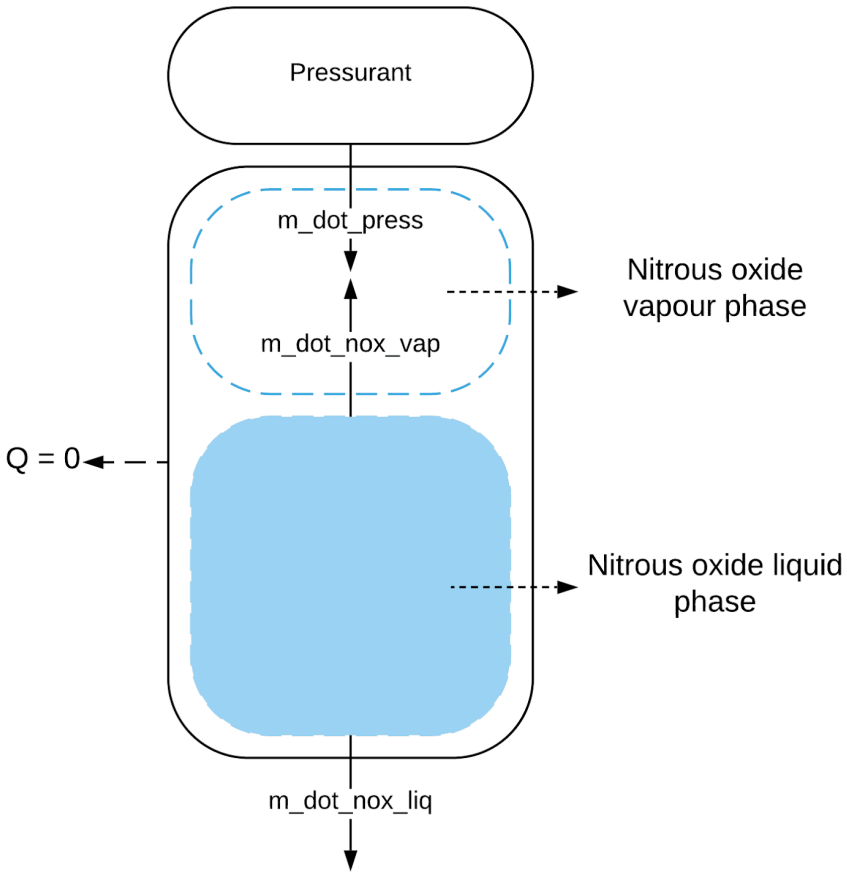

Figure 21 - Nitrous Blowdown Physical Setup

There is an infinitesimally thin control volume used to model the equilibrium between the two phases, but it is not included in the diagram. The following diagram illustrates the solution process at each time step in the blowdown process:

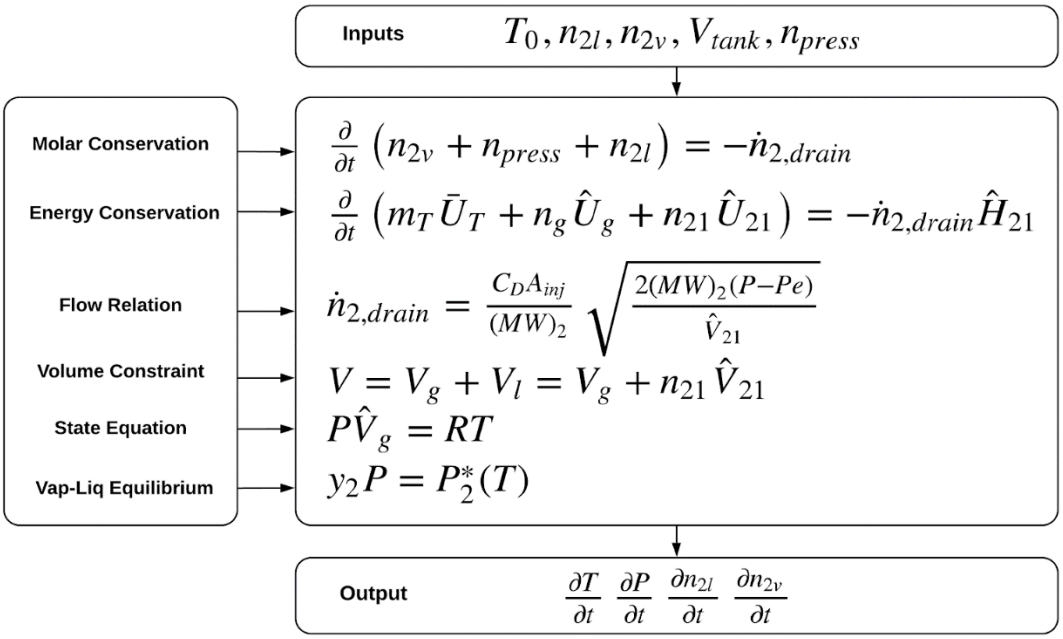

Figure 22 - Blowdown Model Description

Since the outputs are derivatives, any time step can be used to evaluate the change in the temperature, pressure, and amount of liquid or vapour nitrous oxide in the tank (the smaller the better). There are 6 equations required to close the system, and they reflect the assumptions made earlier to simplify the model. The following table describes the inputs and outputs of the model.

Variable	Description
n_2v	Moles of nitrous vapour
n_2l	Moles of nitrous liquid
n_press	Moles of pressurant gas
V_tank	Tank volume
dT/dt	Temperature time derivative
dP/dt	Pressure time derivative
dn_2l/dt	Liquid moles time derivative
dn_2v/dt	Vapour moles time derivative

Figure 23 - Blowdown Model Variables

The blowdown model can accept 3 types of pressurization modes. Those modes result in a differing tank conditions and engine performance during the burn, and thus must be implemented and analyzed separately. The flowcharts for each mode are presented next:

- Constant nitrous oxide tank pressure (left)

  Add enough pressurant at each time step to maintain the pressure in the nitrous tank

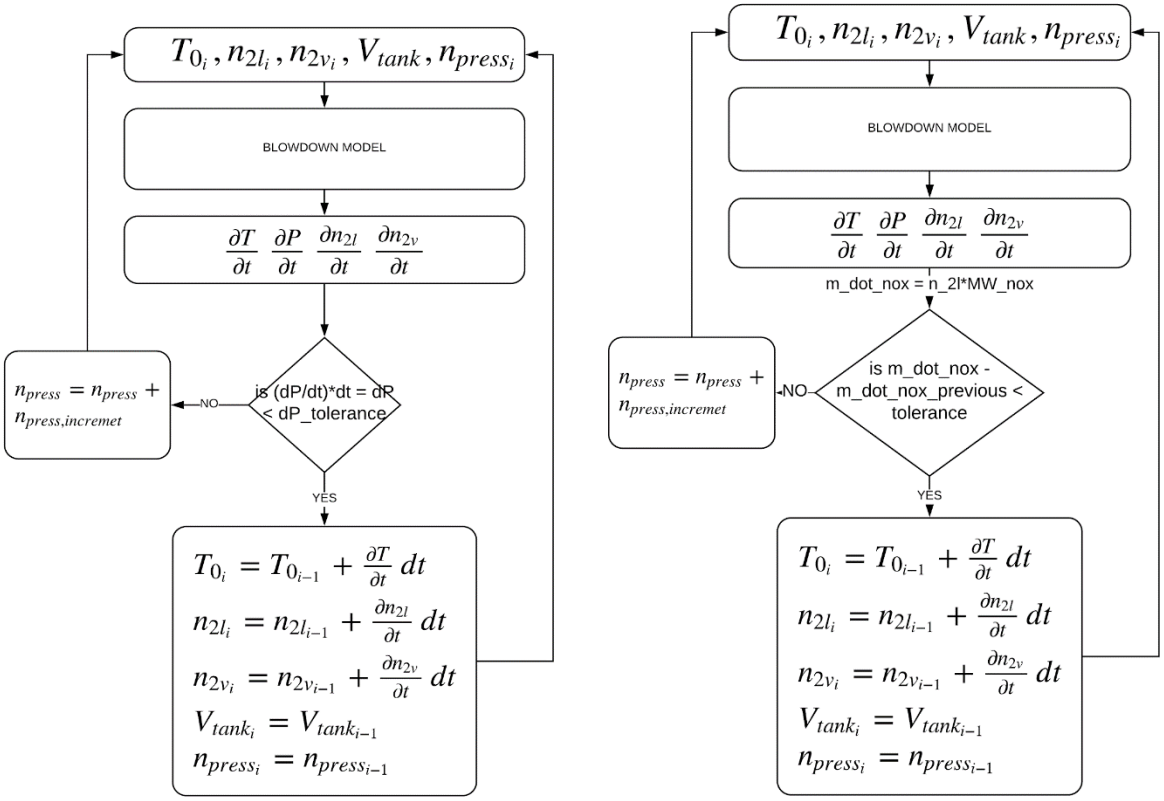

Figure 24 - Constant nitrous mass flow rate mode (right) and constant nitrous oxide pressure mode (left)

- Constant nitrous oxide mass flow rates (right)

  Add enough pressurant at each time step to maintain the desired nitrous mass flow rate out of the tank

- Constant pressure mass flow rate, initialized at time *t* after blowdown start

  Start adding a constant mass flow rate of pressurant into the nitrous tank, t seconds after the blowdown starts

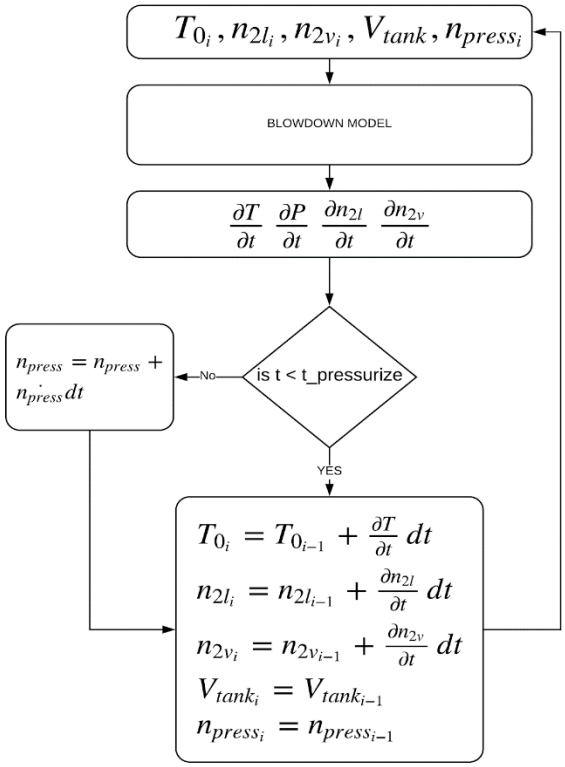

All of these modes start at a specified mass flow rate, then perform their function. A set of tolerances are prescribed to the model for convergence, those can be changed in order to increase accuracy, however, computational time also increases.

Simulation results

The nitrous oxide pressure shows the expected drop over the burn time. This is because of the drop in vapour pressure due to expansion cooling over the blowdown process. The pressurization is performed not to maintain tank pressure, but to maintain nitrous oxide mass flow rate through the injector. In order to keep the mass flow rate constant, a pressure drop is required to balance the temperature drop, since they act in opposing directions.

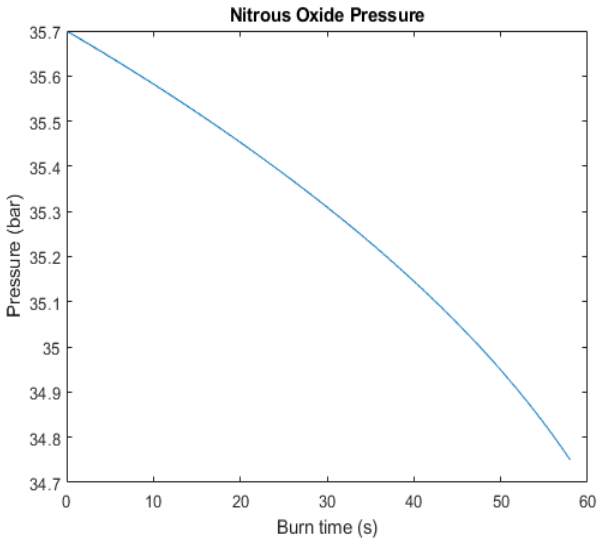

Figure 25 - NOX Pressure Profile

As mentioned previously, the temperature will drop across the burn, because energy is leaving the system as the nitrous blowdown takes place. This temperature drop is also related to the tank materials and their thermal conductivity, as well as the external flight conditions (thermal convection due to flight, and thermal conduction due to aero-heating near hypersonic speeds). During the detailed design phase, those effects will be included in the blowdown model. However, due to the low thermal conductivity of carbon composites, it is expected that the effects from the aforementioned effects will be, although non negligible, small, and will not result in major design requirement changes.

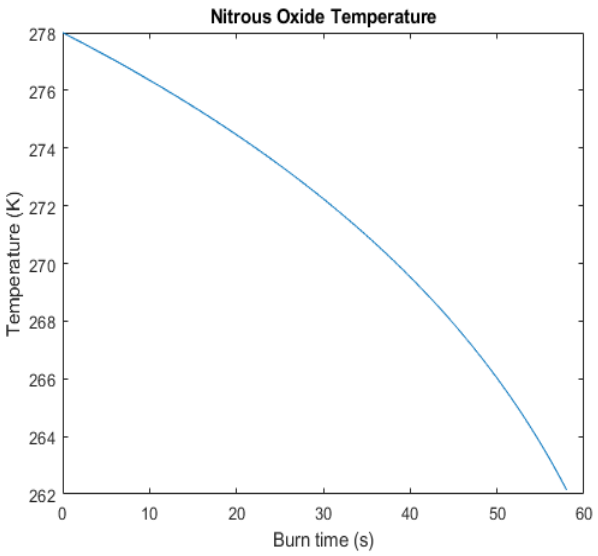

Figure 26 - NOX Temperature Profile

The mass flow rate is maintained constant to within a tolerance of 10e-5 kg/s. The observed mass flow rate drop in the plot is a result of that tolerance, and can be neglected. Maintaining a constant mass flow rate is beneficial for injector design, since injectors can be geometrically optimized for providing a specific mass flow rate.

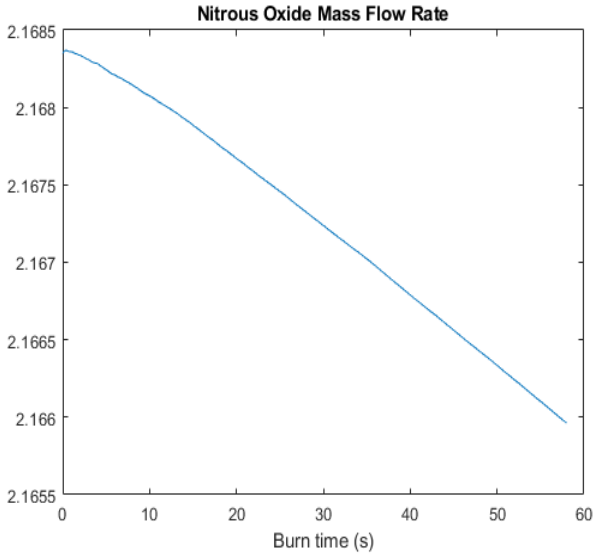

Figure 27 - NOX Mass Flow Rate Profile

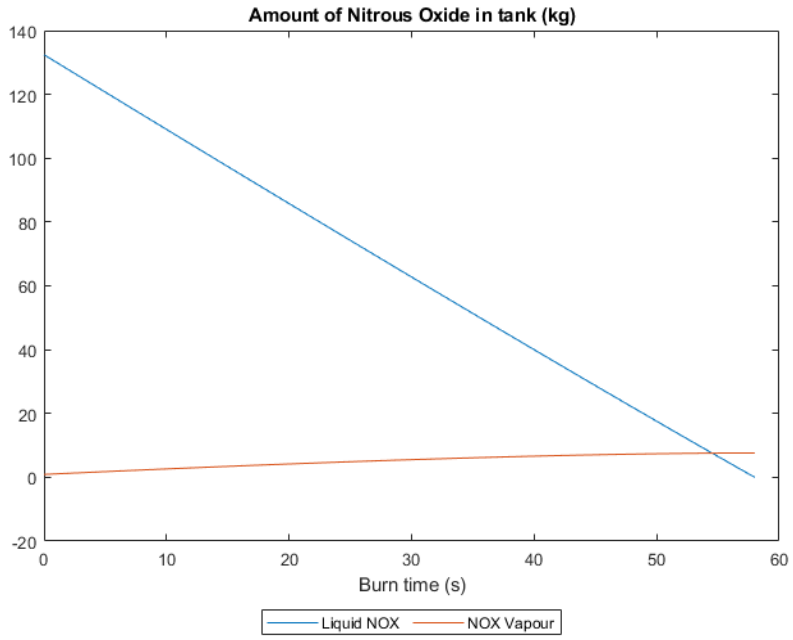

Figure 28 - Amount of NOX in tank during burn

The amount of liquid nitrous and vapour nitrous are shown in the previous diagram. The liquid amount if clearly zero at the end of the burn, however, the amount of vapour nitrous is around 8 kg, due to the evaporation that happens during blowdown. This vapour is responsible for the self pressurization capability of nitrous.

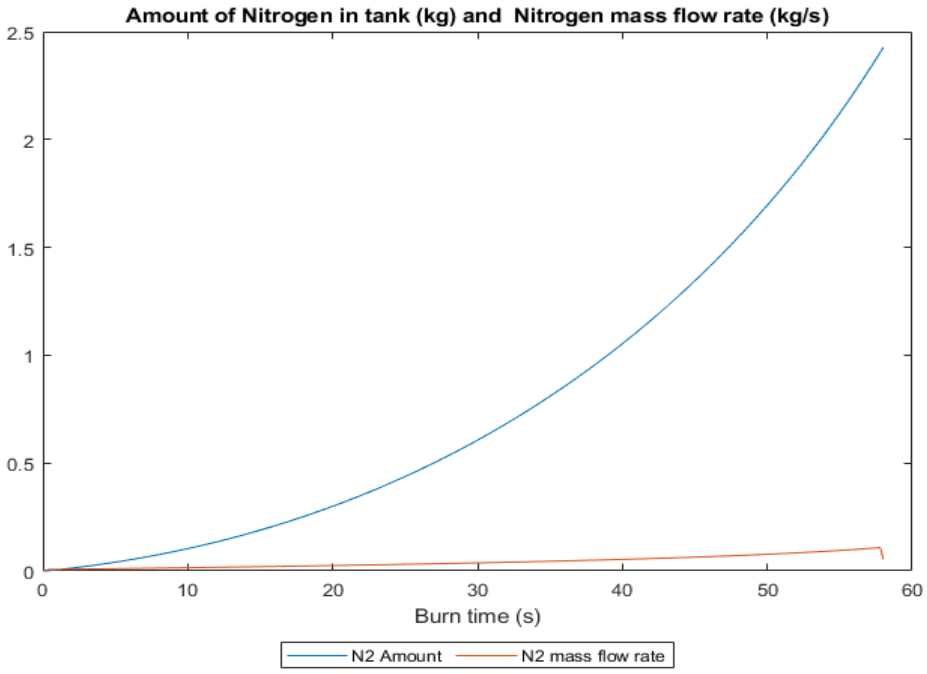

Figure 29 - Amount of nitrogen required in tank during burn

This plot shows the amount of nitrogen pressurant required in the tank throughout the burn, and the associated mass flow rate at all times. Notice the almost linear increase in mass flow rate into the tank. Also notice the small overall values of mass flow rate required.

Testing Plan

Verify Oxidizer Mass Flow Rate

The flow velocities for both propellants were estimated through Bernoulli's Principle. While this may be a reasonable approach for the fuel (ethanol), whether this accurately models the conditions of the oxidizer (N_2O) remains to be seen. For N_2O to follow the behaviour required of Bernoulli's Principle, it must be fully liquid and operate with minimal cavitation throughout the plumbing. While the pressure drop was estimated and the N_2O is not expected to drop below its vaporization pressure, the resulting performance can only be reliably determined through testing.

Since using N_2O to perform cold flow testing is too dangerous, the team will use carbon dioxide (CO_2) as an inert gas substitute. This is common practice among N_2O hybrid rocket cold flow testing as the thermophysical properties of the two fluids are very similar [17].

In terms of measuring the mass flow rate, the team will likely use a flow meter to determine the mass flow rate of liquid CO_2 assuming CO_2 remains full liquid. In the event the CO_2 flows as two-phase flow, the team will elect to expand it to fully gaseous flow through enlarging the plumbing diameter gradually and then use a flow meter to determine the mass flow rate of the gas. The reason being, flow meters do not work under two-phase flow conditions but have proven to be fine with either fully gaseous or liquid phases.

Verify Pressurant Mass Flow Rate

The N_2 will be operating under supercritical conditions, in which case, our current modelling assumptions break down. The selected plumbing diameter for the pressurant was selected to be orders of magnitude higher than the estimated need in order to stack contingency for reaching the necessary mass flow rate. However, a flow constrictor will now be added prior to pressurant being injected into the fuel and oxidizer tanks as a means of controlling the mass flow rate. Calibrating the constrictor can only be done through testing.

To verify the effects of the supercritical pressurant on the flow system, the team can either try measuring the mass flow rate of the propellant itself or measure the resulting mass flow rate of the propellants (dependent variable) in a cold flow test with the pressurant flow constricting orifice as the independent variable. The testing fluid would simply be the nitrogen itself. As it's an inert gas, there's no ignition risks to it. However, the risks from it being a highly pressurized fluids are high in this case.

Operational & Leak Testing

The goal for operational testing is to determine the reliability of the team's on-board valves (main lines, dump, fill), pressure sensors, and pressure reliefs. This testing campaign must be done prior to any cold flow testing that requires the operation of these components.

As an initial step, the team will first perform component level testing on the individual valves and sensors in an easily controlled environment. This will be done post-procurement of components and with the same requirements as if it were an actual cold flow test. Once the components are deemed to be in working conditions, the team will proceed with system level testing. At this final step of testing, the plumbing and components will be fully assembled and pressurized either with or without the combustion chamber. The goal for this is to verify the working order of the components under pressurized conditions as well as to spot leaks in the assembled system as well. Leak detectors will be applied to all separable interfaces.

Verify Tank Pressure Capacity

Both propellant tanks will be tested up to burst pressure for qualification. These tests will be executed by our supporting company PEAK technology which is a professional pressure system manufacturer. The pressurant tanks will be either some certified commercially tanks off-the-shelf or also be qualified by PEAK.

Injector

Injector Type

One of the primary components in a rocket propellant system is the injector system. The injector system delivers both the gaseous oxidizer and liquid propellant into the combustion chamber during engine burn. It is important that the injector system can both mix and atomize the propellants in order to achieve a high degree of flame stability and overall performance. The danger of low mixing and low atomization is that it could lead to localized spontaneous combustion. It is also necessary that combustion is contained within the combustion chamber, and ignition within the injectors are avoided at all costs. In this trade study, we consider three main types of injectors: coaxial, impinging and swirling injectors. The following table shows the weights assigned to the design values for injector trade studies.

Table 38 - Injector Philosophy Criteria Evaluation

Criteria	Safety	Simplicity	Cost	Reliability	Performance	Robustness	Score
Safety		1	1	1	1	1	5
Simplicity	0		0	0	0	1	1
Cost	0	1		0	0	1	2
Reliability	0	1	1		1	1	4
Performance	0	1	1	0		1	3
Robustness	0	0	0	0	0		0

Coaxial Injector

Common types of coaxial configurations are considered in this section. Coaxial injectors consist of overlapping concentric tubes. One of the tubes (usually the inner) contains the oxidizer, while the other contains the fuel. Coaxial injectors typically have good stability characteristics [B]. By swirling the liquid oxidizer, mixing can also be improved [B]. Coaxial injectors tend to produce excellent atomization but are difficult to manufacture and install if several are used [A]. Due to the large number of items compared, a scale of 1-4 is used instead of +/-, with 4 being the best score. Please note that scores across tables cannot be compared, as this first trade study is to compare injector designs within a category with others of that category, before a second trade study comparing the most viable designs of each category.

Table 39 - Coaxial Injector Evaluation

Injector Design	Multiple Concentric Tubes	Multiple Concentric Tubes + Swirler	Multiple Pintles	Single Pintle
Safety [18]	3	3	3	3
Simplicity [19]	2	1	2	3
Cost [20]	1	1	1	3
Reliability [21]	3	1	2	3
Performance [22]	1	3	3	2
Robustness	3	3	3	3
Weighted Score	34	31	36	42

Overall, a single pintle injector appears to be the most pragmatic of the coaxial configurations. The nature of pintle injectors allows for good performance characteristics at relatively high mass flow, without requiring multiple injection orifices. This makes them extremely easy to manifold, as having multiple orifices would require plumbing to each orifice. It is also important to note that pintle injectors are widely used and studied in rocketry applications; thus, it can be asserted that they are generally a reliable injection mechanism.

Impinging Injectors

In this section, we consider differing configurations for an impinging injector element. Impinging injectors operate by injecting streams of fuel and oxidizer through orifices machined into the injector face. Two or more streams of fuel and/or oxidizer collide at an impinging point, where they atomize, and mix in the case of unlike elements. This study is conducted under the assumption that the injector will operate using a singular mechanism specified under this list.

Table 40 - Impinging Injector Evaluation

Injector Element	Like Doublets	Unlike Doublets	Unlike Triplets	Unlike Pentad (Quintuplet)	Showerhead
Safety [18]	4*	3*	3*	2*	4
Simplicity [19]	4	3	3	2	4
Cost [20]	4	3	3	2	4
Reliability [21]	2**	2**	3*	4*	1
Performance [22]	2	3	3	4	1
Robustness	3	3	3	4	4
Weighted Score	46	38	45	44	37

*Risk of blow-apart is characterised under safety instead of reliability, reliability is based on consistency of atomization/mixing.

**Sensitive to design tolerances and changes in flow rate.

Overall, two configurations stand out: the like doublets and the unlike triplets. Although the unlike pentad achieves a similar score, the increase in performance over the unlike triplet is likely marginal, and the unlike pentad configuration itself has a very poor design heritage compared to the other two. Additionally, while the like doublet is a safer design, the blowout risks are largely associated with hypergolic propellants (though the mixture at the impinging point does make damage to the injector plate from combustion instabilities more likely). However, the like doublet has a much stronger design heritage [22] than the unlike triplet, so it is likely the best of the purely impinging designs.

However, the showerhead is not to be written off entirely at the conclusion of this study, which considers injector designs composed of a single type of element. The poor mixing characteristics of the showerhead can be compensated for by deploying it in conjunction with a swirl injector, and the simplicity and excellent wall-compatibility of the showerhead makes it practical to do so in a coaxial arrangement about the swirl injector. Additionally, our team (UTAT) has had experience working with showerhead designs in hybrid rockets, with a sophisticated understanding of the mass flow characterization of plain orifice injectors (see [s15]). Thus, development time and costs can be greatly reduced by incorporating the showerhead injector into a coaxial design.

Premixed Injection

Premixed injection was briefly considered as a possible injection system alternative since nitrous and ethanol are soluble in each other and would produce an ideal premix solution. However, premixed injection is not a well studied mechanism, primarily due to its lack of generality in injection systems and potential safety issues. For example, for hypergolic propellants, premixed injection is not an option as there is no known way to delay combustion from occurring in the injectors. For non-hypergolic propellants, it is possible to prevent combustion from travelling up the injector line by choking the flow at the injector outlet, but this would still pose a safety hazard as the upstream

pressure would have to be constantly maintained; any pressure drop across the injector could result in ignition in the injector, especially with the proposed fuel-oxidizer combination. Another possible solution to this is to restrict the flow area of the injector enough to quench the flame to prevent premature ignition, but this would in turn restrict the mass flow – thereby starving the engine of enough fuel to produce sufficient thrust.

Swirl Injectors

Swirl is a common flame stabilization method in many combustion applications. The fundamental operation of swirling injectors is to introduce rotationality into the fuel flow in a chamber before discharging the fuel into the combustion chamber as a conical sheet where the surface instability of the fluid or a collision with another stream or jet causes the fuel to atomize. A single swirl injector could be used in smaller applications or an array of swirlers could be distributed over a manifold similar to a showerhead or impinging injector design. Swirlers can also be used in conjunction with other types of injector orifices to create a pintle-like configuration; for example, the radial flow from a swirl injector could be combined with axial jets to achieve mixing and atomization in the region of intersection. Two swirlers configured to have different spray cone angles could also be configured to achieve a similar result when the sheets collide. This can be particularly useful on small rocket engines, where the difficulty of accurately drilling small diameters holes can be avoided since, in general, for the same mass flow rate a swirl injector will have a lower discharge coefficient than a jet injector, which translates into larger flow passage area since

$$A = \frac{\dot{m}}{C_d\sqrt{2\rho_l \Delta P}}$$

Table 41 - Swirl Injector Evaluation

Injector Design	Pressure-swirl	Stator Blades	Swirl Vanes	Pre-swirler
Safety [18]	3	3	3	1
Simplicity [19]	4	1	3	1
Cost [20]	4	2	2	3
Reliability [21]	3	3	3	1
Performance [22]	3	2	3	3*
Robustness	3	2	3	1
Weighted Score	48	38	45	25

*Pre-swirlers have not been implemented so performance characteristics are unknown and inferred.

The simplest type of swirl injector is the pressure-swirl injector. The fuel enters a cylindrical swirling chamber through inlet ports tangential to the sides of the chamber and produces a vortex flow with a central air core due to the high rotational velocity of the fluid. The stability of this air core is primarily a function of the inlet tangential velocity, inlet Reynold's number, pressure drop, aspect ratio, and swirl number. The swirling chamber may converge before the flow reaches the discharge outlet and forms a hollow conical swirling film whose spray cone angle is governed primarily by the injector constant K, a function of the injector's geometry. The film then experiences breakup and atomization. Break up is primarily due to the growth of the unstable wave at the interface between the gas and the liquid film and the length over which this breakup occurs is influenced by the liquid film velocity, the gas-liquid relative velocity, the backpressure, the gas density, the liquid density, the surface tension and the spray cone angle. Further atomization of the fluid can be estimated through statistical analysis of the velocity and mass flow distributions. The breakup and atomization of the fuel are also heavily impacted by the high back pressure and temperature of the downstream combustion chamber, which can lead to the fluid film reaching supercritical conditions and changing the mechanisms for which break up and atomization occur. [22]

Like the pressure-swirl injector, a swirl vane injector produces a conical fluid film by producing a rotational flow in a swirl chamber. However, instead of entering the chamber tangentially, the fuel flows axially towards the chamber

but is redirected by a grid of airfoils before entering the swirl chamber. Similarly, stator blade injectors use single or multiple sets of angled airfoils to induce swirl into the fuel before exiting the inject tube and atomizing in the same method as the Pressure-swirl injector. For this project, the size of the rocket engine would require the costly fabrication of small and precise airfoils and vanes with little to no significant gain in performance or stability over the Pressure-swirl injector to justify the higher cost and complexity.

Top Candidate Designs

From each of the classes of injectors, we can select the most optimal design to cross compare their characteristics. These candidates are single pintle, like doublet impinging, and the pressure swirl - showerhead configuration.

Table 42 - Comparison of Top Candidate Injector Designs

Criteria	Weight	Single Coaxial Pintle	Like Doublet	Pressure Swirl - Showerhead
Safety	0.33	-	+	-
Simplicity	0.07	+	-	+
Cost	0.13	+	-	+
Reliability	0.27	+	-	+
Performance	0.20	+	-	+
Robustness	0	+	-	+
Total:		0.67	0.33	0.67

To supplement these rankings based on trade study research, some preliminary calculations need to be conducted to assess the feasibility of each design with the proposed fuels and performance requirements. These will determine if any of the injector configurations would not meet the performance requirements or would require geometries that are too difficult to manufacture.

Proposed Design

Of the top injector candidates from the previous table we decide on the Pressure Swirl - Showerhead injector, where a pressure swirl injector element will be surrounded radially by showerhead injectors in a pseudo-pintle configuration. The pressure swirl element will be injecting the fuel and the axial elements will be injecting the oxidizer. This design balances the high performance provided by the pressure swirl injector and the low development time provided by using the proven axial injectors. As was noted in the Impinging Injector Evaluation table above, utilizing showerhead injectors for both the fuel and oxidizer will result in poor mixing and therefore poor reliability and performance. This problem is mitigated as the sheet from the pressure swirl atomizer will intersect and cause both streams to atomize.

A total of 29, 1.93 mm diameter, showerhead injectors were determined to be needed to provide the total oxidizer mass flow rate at our operating conditions. In order to place all the showerhead elements around a single swirl injector, the showerhead elements would have to be significantly far away from the center element in order for them not to intersect. Therefore, a feasible solution is to increase the number of swirl elements in order to reduce the number of showerhead elements surrounding each one. The final design features 5 swirl elements injecting Ethanol and 6 showerhead elements surrounding each swirl element, injecting N_2O. The total number of showerhead elements is thus 30.

The resultant design can be seen in the following pictures,

Figure 30 - Injector as seen from the combustion chamber

Figure 31- Injector as seen from the combustion chamber, second viewpoint

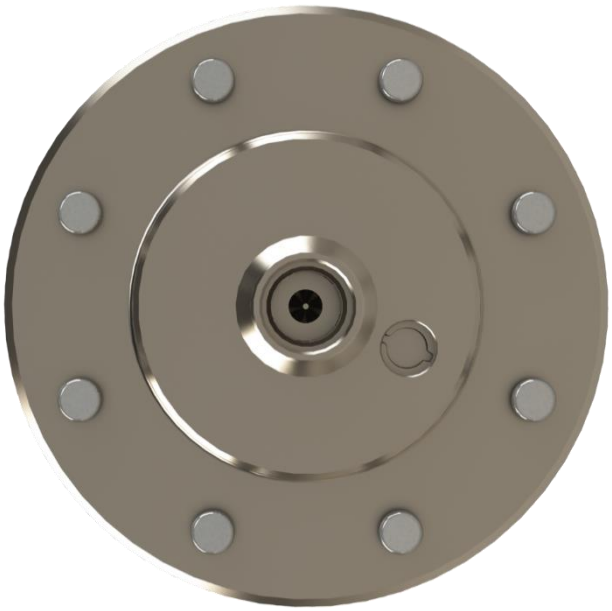

Figure 32 - Injector manifold inlet as seen from the propellant tanks. Pictured is the inlet for the N_2O and Ethanol lines

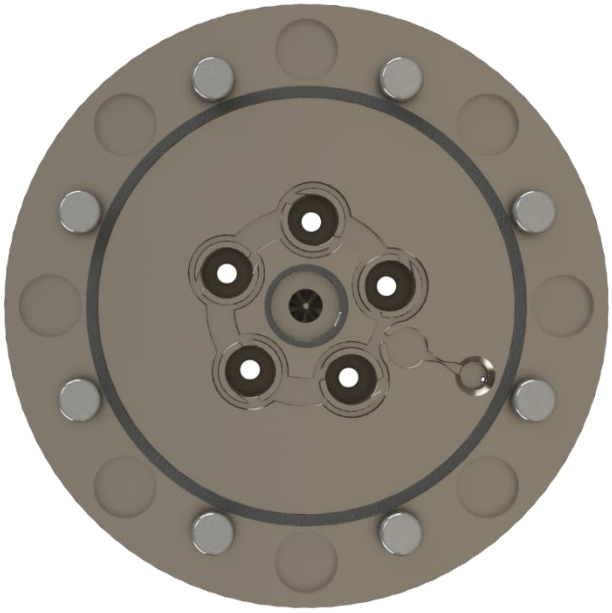

Figure 33 - Middle Injector layer. Pictured are the pressure swirl elements which inject Ethanol.

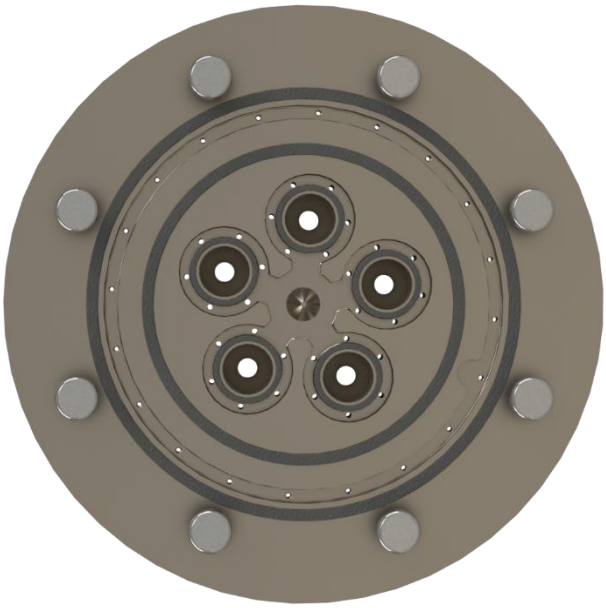

Figure 34 - Bottom Injector layer. Pictured are the showerhead elements which inject N_2O and additional elements used for film cooling the combustion chamber.

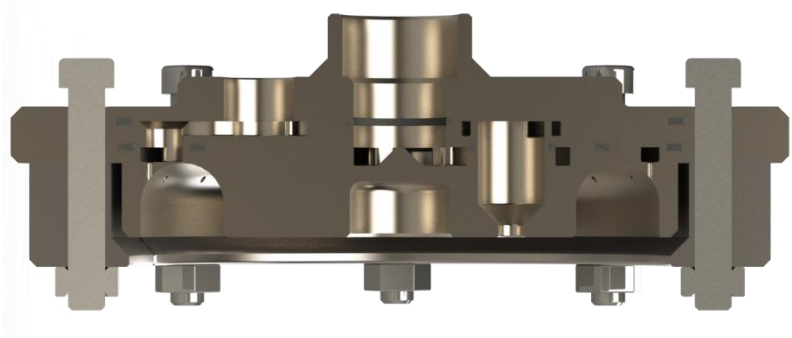

Figure 35 - Cross sectional view of injector. Pictured is the cross section of a pressure swirl element.

As seen from the images above, the injector is divided into a number of individual layers, which act to manifold the flow, and the entire structure is fixed together with a number of bolts.

The injector straight orifice elements' (showerhead) geometric and performance properties are summarized in the following table.

Table 43 - Showerhead Component Properties

Parameter	Value
Inlet Diameter, d (mm)	1.93
Number of Inlets, N	29
Inlet Length-to-Diameter Ratio, L/d	10
Inlet Curvature, r/d	0.05
Exit Velocity, u (m/s)	27.9

Spray Weber Number, We	9.48E+4
Reynolds Number, Re	4.63E+5
Ohnesorge Number, Oh	6.64E-4
Breakup Time (s)	4.59E-4
Breakup Length (mm)	12.83

The injector pressure swirler elements' geometric and performance properties are summarized in the following table.

Table 44 - Pressure Swirler Component Properties

Parameter	Value	Parameter	Value
Spray Angle, θ (°)	40	L_s/D_s	0.7
$C_{d,0}$	0.388	L_P/D_P	1.2
d_0 (mm)	3.70	$A_P/(d_0D_s)$	0.489
l_0 (mm)	1.85	D_s/d_0	2.5
D_s (mm)	9.24	u_p (m/s)	13.08
L_s (mm)	6.47	Re_p	16,000
$C_{d,p}$	0.249	Flow Number, FN (mm^2)	5.88
A_P (mm^2)	16.71	h_0 (mm)	0.470
Number of Inlets	6	u_0 (m/s)	25.7
D_P (mm)	1.88	Sauter Mean Diameter, d_{32} (μm)	6.85
L_P (mm)	2.26	We_0	148,000
X	0.457	Re_0	81,000
A_a (mm^2)	2.24	Oh_0	0.00475
l_0/d_0	0.5	L (mm)	5.10

Analysis

Non-dimensional numbers

Three non-dimensional numbers will be used to evaluate the candidate designs: the Reynolds number, Weber number and Ohnesorge number. The Reynolds number is the ratio of the inertial fluid forces to the viscous fluid forces while the Weber number is the ratio of the inertial forces to the surface tension. The Ohnesorge number relates all three forces as:

$$Oh = \frac{\sqrt{We}}{Re} \sim \frac{viscous\ forces}{\sqrt{inertia \cdot surface\ tension}}$$

Reynolds number:

Indicates the flow regime of the fluid, laminar or turbulent, and can be used to compare how prone the bulk fluid flow is to break up into droplet. The higher the Reynolds number, the more dominate the inertial forces are at overcoming the viscous forces holding together the fluid and the result is complete atomization closer to the exit orifice.

Weber number:

Measures the relative importance of the inertial forces versus the surface tension of the droplets or thin film and is the main quantity that determines droplet breakup mechanisms and the resulting reformation of droplets. With a higher Weber number resulting in a single droplet breaking up into a larger number of smaller droplets.

Ohnesorge number:

Indicates a greater influence of viscosity and describes the tendency for a drop to either stay together or fly apart. Low Ohnesorge numbers are associated with weak friction losses with most of the inserted energy being converted to surface tension energy whereas high Ohnesorge numbers are dominated by internal viscous dissipation. The Ohnesorge number can be used to indicate where the Reynolds number is sufficiently high to achieve complete atomization.

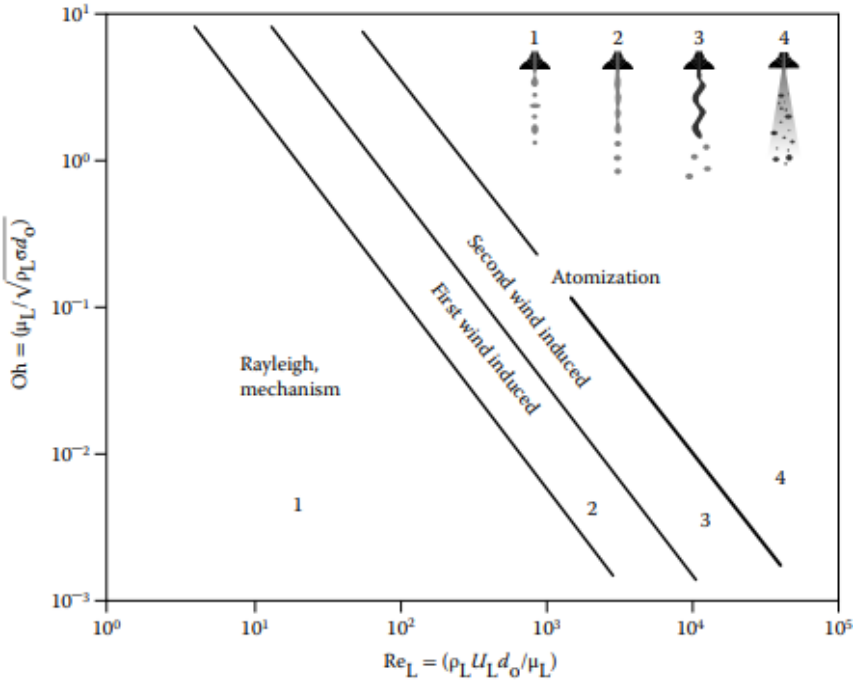

Figure 36 - Classification of Modes of Disintegration/Break-up [23]

Sauter Mean Diameter:

In spray combustion research, the most valuable mean droplet diameter to study is the Sauter mean diameter d_{32} [s13]. In general, small droplets are desirable to facilitate atomization as well as ensure combustion stability. However, injectors do not produces uniform drop sizes for any given operating condition. Thus, the Sauter mean diameter is the most valued, as it is the diameter of a drop whose volume-to-surface ratio is equal to that of the entire spray. This gives important information in situations where surface area is an important consideration, notably combustion processes. Our results have shown that the pintle injector produces droplets with the smallest such Sauter mean diameter, and it is a known high-performance injector type.

Residence time:

It is of interest for a droplet within the combustion chamber to rapidly evaporate in order to improve mixing and combustion characteristics. Shorter residence times also reduce the risk of wall impacts of the droplets. These concerns [s14] make residence time an important metric to consider in the atomization of sprays. The high speed and narrow spray of the showerhead injector allow for a very short residence time in comparison to the swirler injector, although the high-speed spray consequently also means that the breakup length is greater. Currently residence time information is not available for the pintle injector.

Breakup length

Breakup length is the total length from the injector orifice required for the flow to become fully atomized. After the flow becomes atomized, it must be evaporated before it can be combusted. Since this evaporation process is not

instantaneous, there must be sufficient room for evaporation to occur in the combustion chamber. Generally, a shorter breakup length is desirable to leave enough room for evaporation to occur in combustion chambers with limited length.

Cone angle

Cone angle or spray angle is the total angle that the spray forms after exiting the injector orifice. Different spray angles are associated with different performance characteristics depending on the type of injector. The importance of spray angle in injector design is that it is subject to the geometric constraints of the combustion chamber. If the spray angle is too wide, the flow will contact the sides of the combustion chamber, which is detrimental to engine performance.

Showerhead

The showerhead injector is an extremely simple design which employs non-impinging streams on the injector face, which emerge from injector elements normal to the face. These elements can be treated as plain-orifice injectors. The showerhead injector enjoys excellent wall compatibility due to the tight downward angle of the streams, and is extremely simple, which allows for it to be combined with other injector types in our design. This is in fact necessary, as the showerhead injector itself does not have any mixing capability for the fuel and oxidizer, and relies entirely on chamber conditions [s16]. These facts are reflected in the injector scores in the trade study, wherein the showerhead excels in parameters such as safety while suffering in performance parameters, which are compensated for by employing the showerhead in conjunction with the pressure swirler.

Symbols used:

$$
\begin{aligned}
u &= \text{velocity} \\
P &= \text{Pressure} \\
\dot{m} &= mass\ flow\ rate \\
\rho_l &= liquid\ density \\
A &= \text{area} \\
\sigma &= \text{surface tension} \\
\lambda &= \text{radial integral length scale}[s9] \\
d_{32} &= \text{Sauter mean diamter} \\
We_i &= \text{Weber Number}(1 \text{ for liquid, } 2 \text{ for gas}) \\
Oh &= \text{Ohnesorge number} \\
Ta &= \text{Taylor number} \\
\alpha &= \text{jet radius} \\
\mu &= \text{dynamic viscosity} \\
B_1 &= \text{breakup time constant}
\end{aligned}
$$

In order to model the atomization performance of the showerhead injector for liquid nitrous, the plain-orifice atomizer model is used to the flow through an individual injector element. The plain-orifice is the most common type of atomizer and can describe the behaviour of an individual showerhead element. Based on the upstream pressure and chamber pressure, the mass flow rate for an individual 1.93 mm diameter orifice is obtained in accordance with the findings in [s15]. A number N of elements is chosen such that the desired overall mass flowrate is obtained. Additional geometric characteristics (L/d and r/d) are chosen in accordance with [s7]. Velocity is then calculated as a function of the mass flow rate, density, and area: $u = mA$. The Weber number is calculated as:

$$We_1 = \frac{\rho_l u^2 \lambda}{\sigma}$$

and the correlation of [s9] is used to calculate the Sauter mean diameter:

$$d_{32} = 133.0\lambda We_1^{-0.74}$$

The order of magnitude is cross referenced with a study on injector weber numbers in [s6]. Further atomization characteristics of the plain-orifice injector are analyzed using the wave breakup model defined in [s10], as the very high Weber number calculated using the above model implies that droplet breakup is dominated by Kelvin-Helmholtz instability. The gas Weber number is calculated according to the chamber pressure, and the Reynolds number is calculated as:

$$Re = \frac{\rho u \alpha}{\mu}$$

From these, the Ohnesorge and Taylor numbers are also calculated:

$$h = \frac{\sqrt{We_1}}{Re}$$

$$Ta = Oh\sqrt{We_2}$$

The Ohnesorge is verified to be within reasonable boundaries by cross-reference with [s11]. Using these dimensionless relations, the maximum growth rate and wavelength v. jet width are calculated using the following relations from [s10]

$$\frac{\Lambda}{\alpha} = 9.02\,\frac{(1+0.45Oh^{0.5})(1+0.4Ta^{0.7})}{(1+0.87We_2^{1.67})^{0.6}}$$

$$\Omega\left(\frac{\rho_l \alpha^3}{\sigma}\right) = \frac{\left(0.34+0.38We_2^{1.5}\right)}{(1+Oh)(1+1.4Ta^{0.6})}$$

The breakup time is then given by:

$$\tau = \frac{3.726B_1\left(\frac{\Delta}{a}\right)^{-1}}{\Omega}$$

where B_1 is set to 1.73 as recommended by [s12].

Pressure Swirler

For the ethanol pressure swirler we must determine the following dimensions and characteristics as shown in the figure below: exit orifice diameter (d_0) and length (l_0), swirl chamber diameter (D_s) and length (L_s), inlet port diameter (D_P), length (L_p), the number of inlet ports, and the spray angle (2θ).

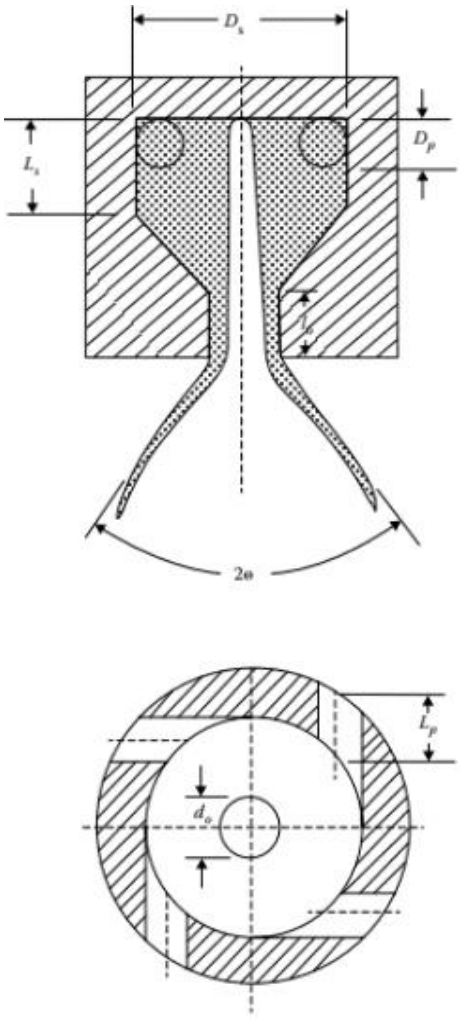

Figure 37 - Pressure Swirl Atomizer Cross-Sections and Dimensions [23]

To determine these parameters, we shall employ the method used by Rezende and Perez [24] which using the exit orifice as a mean to achieve the spray cone angle and the inlet orifice to achieve the desired mass flow rate. First, we pick a desired spray angle, say 45°, and then determine the open area ratio (ratio of central air core area to exit orifice area), X, which can then be used to determine the exit discharge coefficient

$$C_{d,0} = \sqrt{\frac{(1-X)^3}{1+X}}$$

Then using the desired mass flow rate and the definition for hydraulic flow through an orifice the exit orifice area, and then diameter, can be calculated as

$$A_O = \frac{\dot{m}}{C_{d,out}\sqrt{2\rho_l \Delta P}}$$

Next, to determine the inlet parameters, we determine and inlet discharge coefficient

$$C_{d,p} = \sqrt{\frac{(X)^3}{2-X}}$$

Then, using the same hydraulic equation to determine the required inlet area:

$$A_P = \frac{\dot{m}}{C_{d,in}\sqrt{2\rho_l \Delta P}}$$

This area can be divided between multiple inlet ports to obtain an inlet diameter that optimizes other injector parameters. The remainder of the injector dimensions are determined from ratios recommended by Lefebvre and McDonell [23].

Range of Values of Nondimensional Groups Covered by Jones

Dimensionless Group	Range Covered	Typical Value	
$\frac{l_o}{d_o}$	0.1–0.9	0.15	–
$\frac{L_s}{D_s}$	0.31–1.26	0.7	–
$\frac{L_p}{D_p}$	0.79–3.02	1.2	–
$\frac{A_p}{d_o D_s}$	0.19–1.21	0.52	–
$\frac{D_s}{d_o}$	1.41–8.13	2.7	–
$\frac{d_o \rho_L U^2}{\sigma}$	11.5×10^3–3.55×10^5	Low pressure 2.4 MPa (350 psi) 1.08×10^5	High pressure 6.3 MPA (900psi) 3.88×10^5
$\frac{d_o \rho_L U}{\mu_L}$	1.913×10^3–21.14×10^3	6.45×10^3	23.64×10^3
$\frac{\mu_L}{\mu_A}$	279–2235	750	–
$\frac{\rho_L}{\rho_A}$	694–964	700	–

Source: Jones, A. R., Design optimization of a large pressure-jet atomizer for power

Once the dimensions of the swirler are determined, the following performance parameters can be calculated: liquid sheet thickness, break up length, exit tip velocity, Sauter Mean Diameter, and the non-dimensional Reynolds, Weber, and Ohnesorge numbers using the exit orifice conditions.

The liquid sheet thickness at the exit can be estimated [25] by:

$$h_0 = \frac{0.00805 FN \sqrt{\rho_l}}{d_0 \cos\theta}$$

where FN is the flow number

$$FN = \frac{\dot{m}}{\sqrt{\rho_l \Delta P}}$$

The slant breakup length (i.e. along the spray cone) can be empirically estimated [26] using

$$L_{bu} = 0.82 \sqrt{\frac{\rho_l \sigma \, ln(\eta_{bu}/\eta_0) \, h \cos\theta}{\rho_g^2 u^2}}$$

where $ln(\eta_{bu}/\eta_0) = 2.5$. The axial breakup length is then $L = L_{bu} \cos\theta$. The axial exit tip velocity is determined by:

$$u = \frac{\dot{m}}{\rho_l (A_0 - A_a)}$$

and the Sauter Mean Diameter by the empirical equation [27]

$$d_{32} = 0.436\mu_l^{0.55}\rho_l^{-0.74}d_0^{-0.05}A_p^{-0.24}$$

Executing the described methodology and dividing the ethanol flow amongst five pressure swirlers to accommodate the required number of nitrous orifices we arrive at the following

CFD Analysis

Flow Analysis

The use of N_2O as a propellant in a rocket engine can significantly complicate the injector design because it is typically utilized at near-saturated conditions. A saturated fluid, at its vapour pressure, forced through a constrained volume, such as an injector, will experience a drop in pressure and an increased velocity and mass flow rate. As the vapour pressure marks the liquid-gas transition point, the liquid becomes a two-phase mixture. A subcooled fluid can also enter the two-phase region, given a sufficiently large pressure drop. This phenomenon often manifests itself in the form of bubble formation within the flow and is termed cavitation. The fluid across the volume will continue to experience an increase in velocity and mass flow rate as the pressure further drops until the fluid velocity reaches the local sonic velocity. At this point, the flow is said to be choked, the mass flow rate stops increasing and is termed 'critical mass flow rate'. Downstream pressure changes are unable to interfere with upstream conditions as pressure waves are unable to travel upstream because the speed of sound is equal to the rate of propagation of pressure waves.

Analytical Models

Typical two-phase analytical and numerical models fall short of definitively predicting the impact of cavitation. Because of this gap in the literature UTAT has assessed a wide range of two-phase analytical models and developed a new model [1], capable of predicting mass flow rate and critical pressure for axial N_2O injectors with an average error of 3.9% over a wide range of upstream pressures and injector diameters.

The following figure and table benchmark different analytical mass flow rate models against experimental data from Waxman for N_2O. The table utilizes 26 test cases from Waxman, totalling over 2,600 mass flow rate data points.

https://stacks.stanford.edu/file/druid:ng346xh6244/BenjaminWaxmanFinal-augmented.pdf

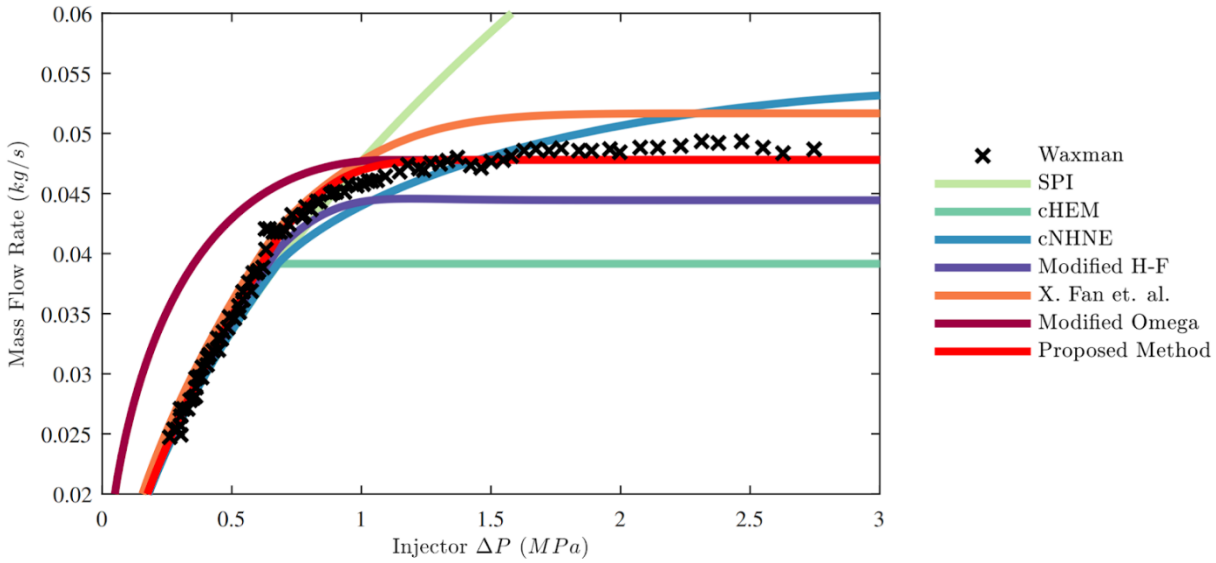

Figure 38- Analytical mass flow rate models compared to experimental data from Waxman for N2O.

Table 45- Error of analytical mass flow rate models predicting experimental data from Waxman.

Injector Diameter (mm)	Fluid	SPI (%)	cHEM (%)	cNHNE (%)	Modified (%) Henry-Fauske	X. Fan (%)	Modified Omega (%)	Proposed Method (%)
0.79	N_2O	7.22	6.79	6.50	3.20	26.10	2.01	6.71
0.79	CO_2	5.92	5.88	5.23	3.55	21.77	3.31	5.06
1.50	N_2O	4.44	3.68	2.73	5.82	14.46	4.24	2.69
1.50	CO_2	4.54	4.62	3.47	6.41	27.39	6.32	2.82
1.93	N_2O	3.25	1.22	1.64	4.80	26.81	10.01	1.97
Mean Absolute Percentage Error		5.07	4.44	3.91	4.76	23.30	5.18	3.85

CFD Models

Low-dimensional analytical relations, such as the aforementioned, are utilized for the purpose of design in order to quickly arrive at a prediction for two-phase mass flow rate through the injector. These models however cannot be used to study the flow over space or time due to their low-dimensional and steady state nature. The presence of cavitation inside a N_2O injector may alter the nominal velocity profile, turbulence level, spray and atomization characteristics [2]. This becomes problematic when modelling spray break-up and atomization processes as knowing the boundary conditions of the fluid at the exit plane of the injector element becomes crucial [3].

In order to solve for the fluid state at the exit plane of the injector, study the flow development along the injector channel and study the mixing between the ethanol and N_2O inside the combustion chamber, we turn to high fidelity CFD simulations. Two-phase fluids are complex phenomenon that can manifest a wide range of properties. As such, the results of a two-phase fluid simulation may vary widely depending on the mathematical models chosen to represent the phenomena they exhibit. Therefore, the correct representation of a two-phase fluid is key to its solution [4] [5].

Common RANS methods for modelling multiphase flows include the one-fluid VOF approach, two-fluid Euler-Euler approach, as well as hybrid methods which combine different approaches. We currently have benchmarked these three CFD methodologies and their ability to predict the cavitation phenomena through the N_2O injector [1]. The open source CFD platform OpenFOAM [6], is used for the entirety of the CFD analysis. As seen in the following figures the predicted mass flow rate error is below 10% for nearly all simulations.

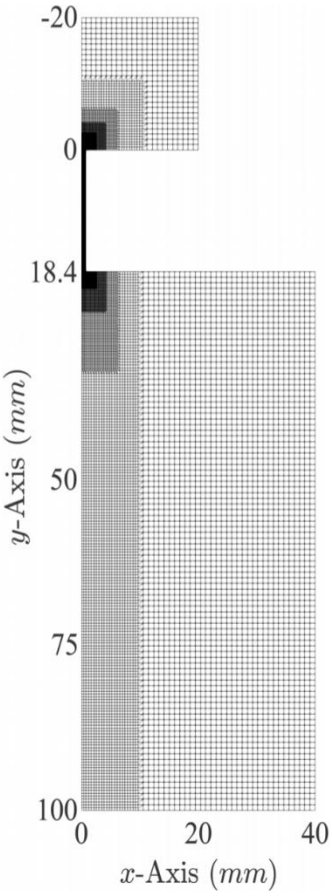

Figure 39 - Injector mesh for CFD analysis

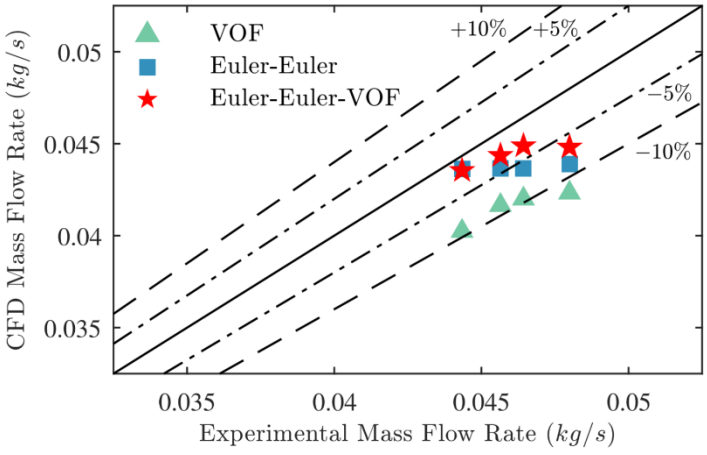

Figure 40 - Mass flow rate error predicted by the three different CFD methodologies

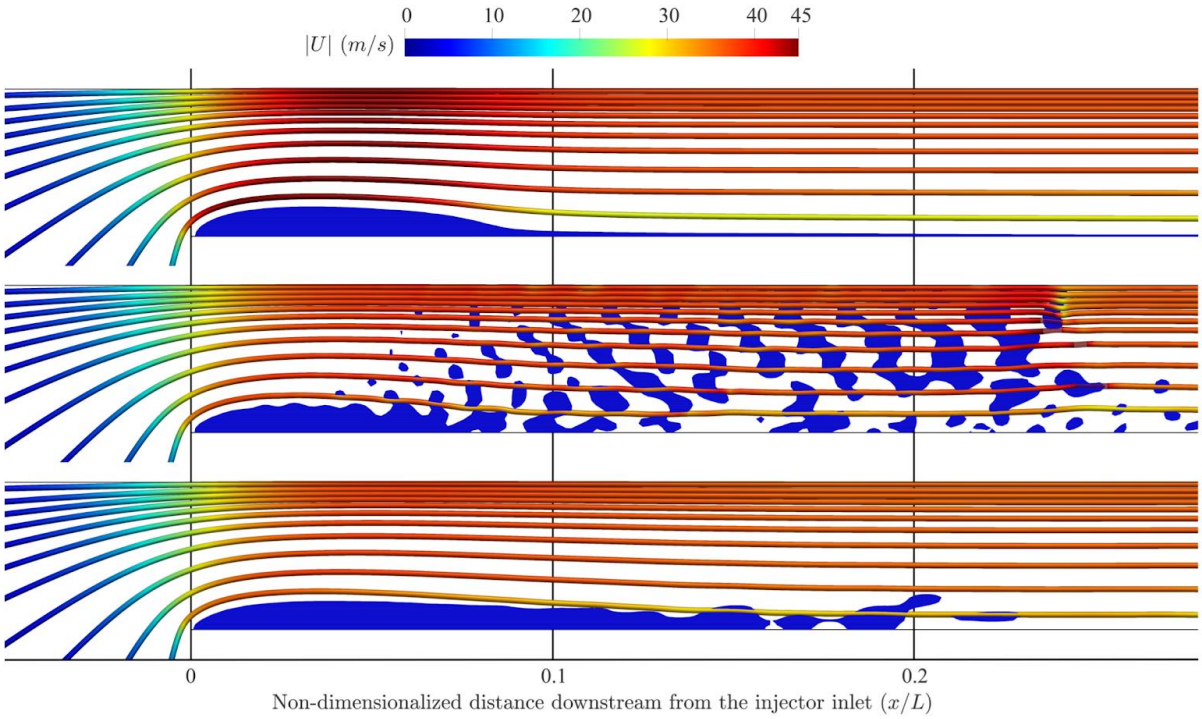

Figure 41 - N2O vapour cavity development as predicted by VOF (top), Euler-Euler (middle), and Euler-Euler-VOF (bottom) CFD methodologies. The streamlines are coloured by velocity magnitude and the liquid phase fraction iso-volume for α = [0, 0.6] is shown in blue

[1] E. Vargas Niño, M. R. Razavi, Design and Testing of Two-Phase Injectors using Analytical and Numerical Methods with Application to Hybrid Rockets, Propulsion and Energy Forum (2019) [Under Review]

[2] Gómez-Aldaraví, Development of a computational model for a simultaneous simulation of internal flow and spray break-up of the diesel injection process, Doctoral Dissertation (2014).

[3] Saha, Kaushik, Ph.D. thesis (2014), http://hdl. handle.net/10012/8628.

[4] G. Cerne, S. Petelin, and I. Tiselj, Coupling of the ˇ interface tracking and the two-fluid models for the simulation of incompressible two-phase flow, Journal of Computational Physics 171, 776 (2001)

[5] S. M. Damián and N. M. Nigro, The detached interphase simulation, Mecánica Computacional 32, 1825 (2013).

[6] H. G. Weller, G. Tabor, H. Jasak, and C. Fureby, A tensorial approach to computational continuum mechanics using object-oriented techniques, Computers in Physics 12, 620 (1998).

Injector testing plan

Testing Scope

The primary focus of the injector testing campaign is broken down into two main streams:

- Model validation tests
- Validating computational and analytical models
- Build confidence in design methodology
- Concept exploration tests
- Showerhead injectors with varying number, position, and cross section of openings.

- Doublet impinging injectors with varying number, position, cross section, and angle of openings.
- Pintle injectors with varying cross sections.
- Swirl injectors with varying cross section and angle of the fuel openings.
- Secondarily this setup will also give us data on the the feasibility of using critical venturis for mass flow regulation.

Toronto Subscale Test Stand

An extensive cold flow campaign for the injector is planned in the coming weeks. The cold flow test setup is currently under construction at the University of Toronto Institute of Aerospace Studies (UTIAS). A 3D rendering of the entire test setup and chamber test section is shown in the following figures. The current setup supports testing of a single propellant at a time.

This cold flow campaign will focus on validating the mass flow models and simulations mentioned in the previous sections. The N2O injector element will first be tested as its behaviour is more difficult to predict than ethanol which will be tested after.

The experiments will serve as a comparison for the prediction of mass flow rate and critical choking pressure. In addition, the study will focus on atomization and stability in the engine by studying the spray angle, droplet size, and other characteristics through shadowgraphy and Schlieren imaging of the spray.

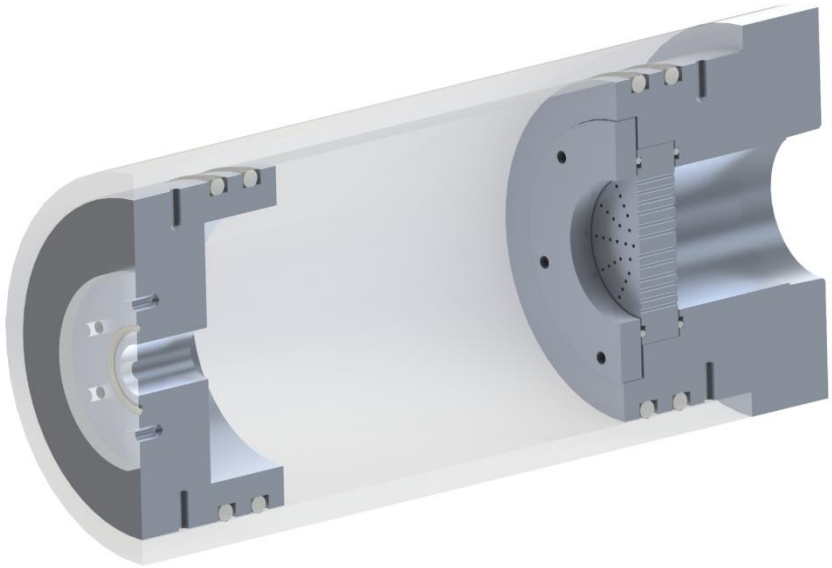

Figure 42 - Cold-Flow test section with transparent acrylic

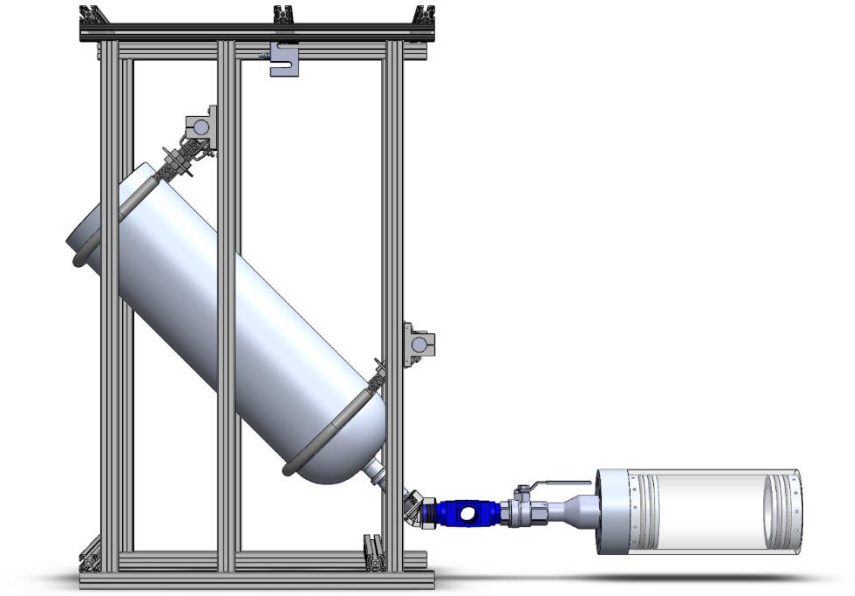

Figure 43 - Cold flow test setup

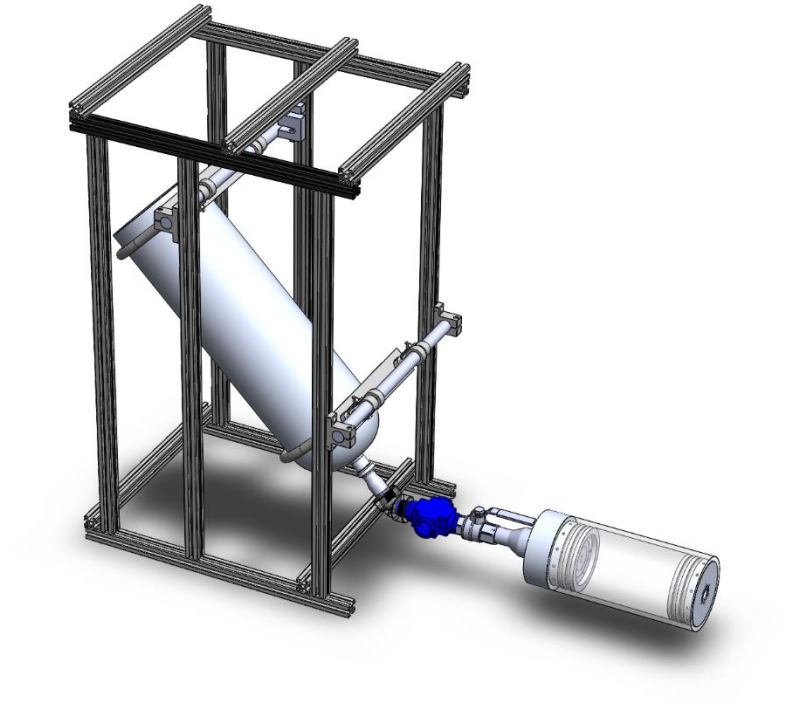

Figure 44 - Cold flow test setup, alternate view

Shadowgraphy

Shadowgraphy is a simple but effective method for capturing the spray pattern of an injector. A flash is placed facing a camera and the fluid spray is placed between the flash and the camera so that it creates a visible shadow. The resulting high contrast image of the spray can be used to verify atomization characteristics such as spray angle, droplet diameter and breakup length.

Schlieren photography

A more refined and complex version of shadowgraphy, schlieren photography utilizes the different refractive indexes that occur for different densities of fluid for imaging. Depending on the refractive index, light will bend at different angles, which can be imaged to see relative densities of fluid. The setup for schlieren is more complicated, a light source is focused on a subject with a convex lens, but the source itself is omitted from the image by placing a razor blade at the focal point. This way, the differences in densities of fluid become more apparent.

Vienna Subscale Test Stand

In order to supplement and verify the calculations and trade studies done to find an appropriate injector concept, a small scale test engine was built. It is based on a pre-existing design built in 2018 but is a lot more modular in order to easily test different injector types and configurations.

In addition, this small scale engine provides an opportunity for our team to practice the operation of a rocket engine under more forgiving conditions than would be the case with a full scale engine.

Specifications:

The engine is configured to use ethanol as fuel and oxygen enriched air (NitrOx) as oxidiser at an oxidiser to fuel ratio of 2.5. It is expected to reach a specific impulse of close to 200 seconds and was designed to deliver 200 Newtons of thrust. The oxidiser system has a working pressure of 20 bar, the fuel system of 30 bar and the engine itself runs at a chamber pressure of 10 bar. For the first round of cold flow tests, to check the functionality of the setup itself, water will be used as a substitute for the fuel and nitrogen in place of the oxidiser.

Configuration:

The test setup consists of several different parts arranged in two main build groups. One group is the test stand itself, including injector, chamber and nozzle, structure, fuel tank, ignition system, and electronic valves. The other group, the control stand, consists of the fuel pressurant and oxidiser tanks, the manual valve setup, and the computer controlling the test sequence. The two groups are joined together by the high pressure hoses carrying oxidiser and fuel pressurant as well as a data cable connecting the computer to the electronics box.

The injector is highly modular. The fuel and the oxidiser sections can be disassembled independently of each other making it possible to switch out parts quickly, enabling rapid systematic testing. To get the conditions inside the chamber as close as possible to the ones encountered when using nitrous oxide, a deceleration chamber was added in the oxidiser line between the regulating venturi and the injector, since the gaseous NitrOx would otherwise have a far higher flow velocity than the nitrous oxide which would be partially liquid at this point and therefore much denser.

In the case of hot fire tests ignition is provided by a high voltage arc between two contacts inside the engine chamber.

The engine is mounted in a steel frame with the nozzle pointing towards the ground. The fuel tank is mounted to the side of the structure, with a piece of sheet steel providing thermal protection from the engine exhaust. Since the hot fire duration of this test stand will never exceed fife seconds this was deemed sufficient.

This plate also provides structural support for the electronics box that controls the valves and the ignition system.

The electronic fuel valve is mounted on the fuel tank while the electronic oxidiser valve is located on top of the injector.

From the fuel tank or oxidiser valve respectively several meters of high pressure hose run to the control stand, which is separated from the test setup by a solid concrete wall. This is to prevent injuries of testing personnel by flying debris in the unlikely event of an explosion.

The two high pressure hoses, carrying NitrOx at 20 and Nitrogen at 30 bar respectively each connect to a 10 litre 200 bar gas bottle via a pressure regulator. Both pressure regulators are equipped with manual safety valves.

The final part of the control stand is a computer running a python script that controls the electronic valves and the ignition system. This will be changed to the LabVIEW software in the future.

Mass Flow Regulation:

To regulate the mass flow of oxidiser and fuel to our engine critical venturi nozzles are used.

On the oxidiser side this is rather straightforward. Since the NitrOx in use is gaseous and thus compressible there exists a minimal ratio between the pressure upstream and downstream of the venturi so that the flow at the throat reaches the speed of sound effectively decoupling the mass flow rate from the downstream pressure, hopefully reducing combustion instabilities. In this state the mass flow rate is only dependant on the upstream density, which itself is directly dependant on the pressure, and the diameter of the venturi nozzle.

For the fuel system things are a bit more complicated since the liquid ethanol is a non compressible fluid. Here a cavitating venturi is used to achieve a similar effect. If the ratio between the upstream and downstream pressure is large enough and the throat of the venturi small enough the pressure at the throat of the venturi drops below the vapor pressure of the ethanol. As a result our fuel turns into a compressible fluid which again enables us to regulate the mass flow.

Operation:

To operate the test stand a computer operator and one person at each pressure regulator are needed. In addition the presence of a safety manager and a dedicated sensors operator are useful.

After the assembly of the test setup the computer operator does an electronics check. This includes opening and closing the electronic valves and activating the ignition. If everything is nominal the sensors operator switches on the camera filming the test, then the whole test crew evacuates the test stand and assumes their positions on the control stand. The fuel and oxidiser operators pressurise the system then the computer operator starts the pre programmed test sequence. In case of irregularities during the test it is either interrupted via the control software or, if the issue is with the electronics, the fuel and oxidiser operators open the manual safety valves cutting off the pressure from the system and depressurising the lines and the fuel tank. After a successful test the pressure is switched of at the regulators, then the lines and tank are depressurised via the manual valves. In both cases the system is then in a safe state so the test crew can approach for reconfiguration or incident investigation and the sensors operator can switch off the camera and write down the sensor readings.

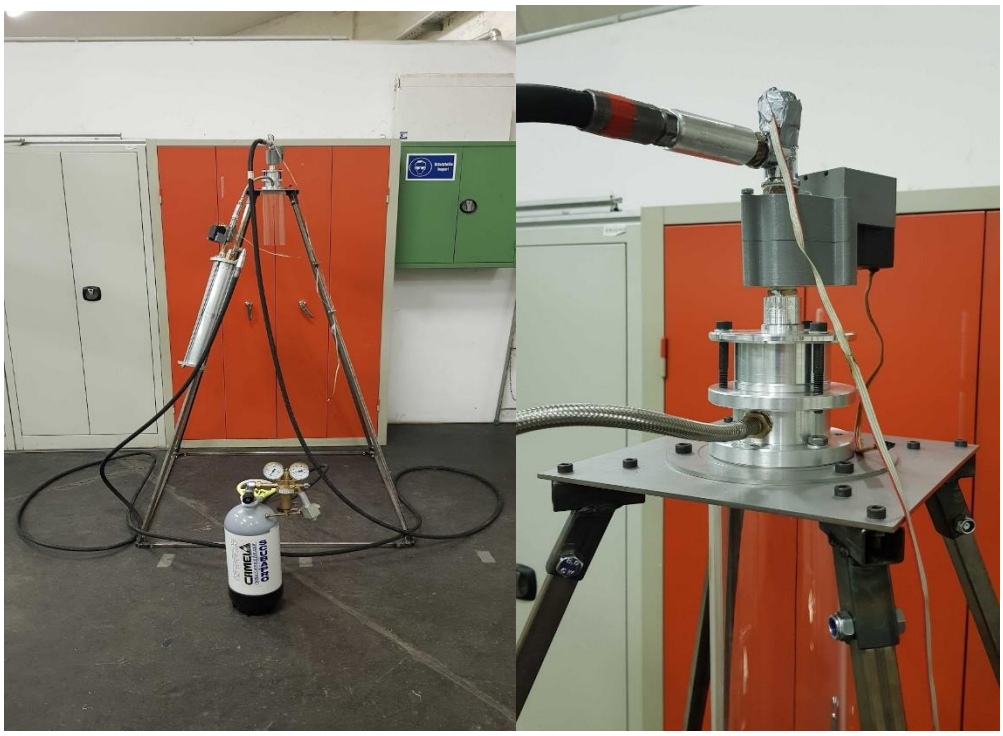

Thrust Chamber

This section details the geometric design of the combustion or thrust chamber of the engine. Simply put, designing a thrust chamber is much like designing a pressure vessel. The main difference is that the diameter and length of the combustion chamber are dictated by the combustion physics of the propellants. The design process for the combustion chamber (i.e., calculation of chamber diameter, length and wall thickness) is described in the following.

First, every rocket engine needs a nozzle throat that is choked. Choking refers to when the flow passing through the throat reaches the speed of sound, i.e., $M = 1$, where M is the Mach number of the gases. From the Continuity Equation/conservation of mass, it is known that the mass flow rate, $\dot{m}$, at any point in the engine must be constant, which has to be equal to the total mass flow rate of fuel and oxidizer. From isentropic relations, one can obtain the following equation relating fluid properties and mass flow rates.

$$\dot{m} = AMP_0\sqrt{\gamma RT_0}\left(1 + \frac{\gamma - 1}{2}M^2\right)^{\frac{\gamma+1}{2\gamma-2}} \tag{2}$$

Where A is the cross-sectional area, P_0 is the stagnation pressure of the gases, γ is the ratio of specific heats, R is the specific gas constant and T_0 is the stagnation temperature. At the throat of the nozzle, we want $M = 1$ and we also assume that $P_0 = P_{cc} = 2{,}416\ kPa$, the combustion chamber pressure. Then, by using NASA's CEA to compute the properties of the combustion products (γ, R and T_0) and rearranging the above equation, we get an equation for the throat area, A_*,

$$A_* = \frac{\dot{m}}{P_{cc}\sqrt{\gamma RT_0}\left(\gamma + 1/2\right)^{\frac{\gamma+1}{2\gamma-2}}} = 0.001730\ m^2 \tag{3}$$

To compute this value, we assumed that the chamber pressure, P_{cc}, was equal to the stagnation pressure of the combustion gases, P_0. This is not normally true, but if the cross-sectional area of the thrust chamber is at least three

times larger than the throat diameter, then $\frac{P_{cc}}{P_0} \geq 0.99$. As a result, both the diameter of the combustion chamber and the nozzle throat are now constrained. Due to the geometry of the system, the diameter was set to 14.1 cm.

The next parameter to compute is the chamber length, L. Rocket engineers use the characteristic chamber length, L^*, as a way of accounting for combustion physics, which includes the effects of droplet vaporization, combustion chemical timescales and fluid flow timescales. There are complicated empirical equations for calculation L^*, but they will not be presented here in the interest of brevity. Spalding's model was used to estimate L^* for the selected propellants and injector design, yielding a value of approximately 2 m [36]. From L^* and the choice of $A_{cc} = 3A_*$, one can compute the optimal chamber length:

$$L^* = \frac{V_{cc}}{A_*} = \frac{LA_{cc} + V_{conv}}{A_*} \Rightarrow L = \frac{L^*A_* - V_{conv}}{3A_*} = 0.205\ m \tag{4}$$

Where V_{conv} is the volume of the converging section of the chamber leading to the nozzle throat. V_{conv} is calculated as the volume of a truncated cone.

Finally, we can compute the wall thickness using thin-walled pressure vessel theory. Setting the safety factor to be 2 at the 2,416 kPa operating pressure gives

$$t = \frac{P_{cc}r_{cc}}{\sigma_y} = 2.6\ mm \tag{5}$$

Where r_{cc} is the radius of the chamber and σ_y is the yield strength of the material. The yield strength was estimated from experimental burst tests of the DragonScale material. The details and results of these tests will be presented in the following section. The diagram below indicates the dimensions of the thrust chamber.

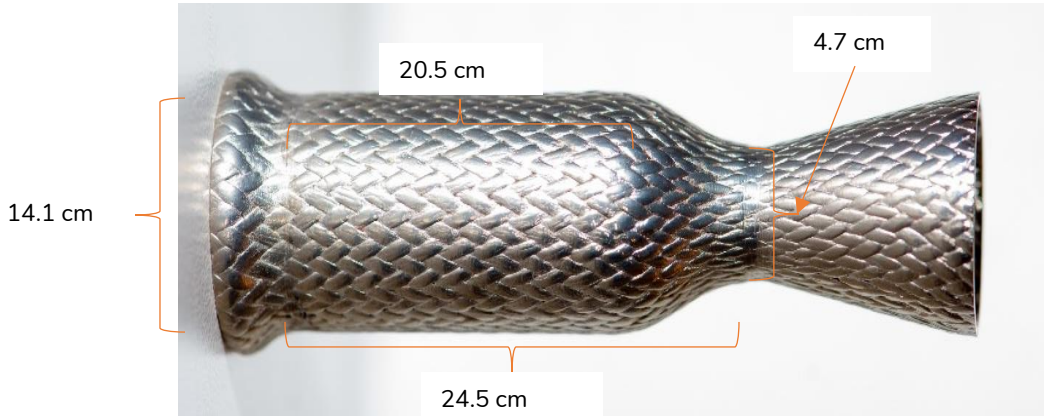

Figure 45 - Sample DragonScale Thrust Chamber with Design Dimensions

Engine Thermal Management

Chamber Cooling Method

The temperatures experienced by high-performance rocket engines most often exceed the melting points of materials strong and light enough to withstand the forces experienced by the thrust chamber. Engines use innovative cooling methods to prevent the thrust chamber from overheating while keeping the mass required for such a cooling system to a minimum. The cooling techniques investigated here are regenerative, radiative and film-based. Regenerative cooling uses some coolant, often the propellants, to absorb the heat of the engine through a heat exchanger, using the absorbed energy to perform additional tasks, such as driving turbomachinery or increasing injection pressures. Radiative cooling enables the engine to dissipate heat as light, without the use of any working

fluid. Film-cooling techniques often use the propellants to coat the walls of the combustion chamber in a thin film which absorbs heat through vaporization.

Table 46 - Comparison of Cooling Methods

Cooling Method	Regenerative	Radiative	Film
System Mass	High	Low	Middle
Manufacturing	More complex	Simple	Middle
Heritage	High	Low	Low
Industry Use	Common	Uncommon	Growing popularity

Although this trade study is a very important one, in our case, one of the main goals of this project is to test and verify the DragonScale material. This has been a goal even before the team was formed, and this the decision to go with the radiative cooling method was made implicitly. It was As a result, this trade study serves more as a guideline for selecting an alternative cooling system if the DragonScale material underperforms in static engine tests. From this trade study, film cooling was selected as the back-up cooling method.

Metal Matrix Composites (MMC)

The aerospace industry has been the driving force for the development of continuous fibre reinforced metal matrix composites (MMCs) in the past. Due to demand for lightweight materials with highly specific requirements the investigation of new composite materials is essential for improvements in the space industry. Continuous carbon fibre metal matrix composites have already found some primary applications in principally structural products, e.g. reinforced beams and light panels exhibiting high strength and stiffness at very low weight. Continuous fibre reinforced MMCs are processed by many different techniques which can be divided into three main approaches.

- The class of liquid metal casted, stirred, injected and infiltrated fibres. These processes are achieving good fibre impregnation due to special pre-coatings. The downside is shrinkage, residual stress and potential fibre damage though fabrication at elevated temperatures.
- Metal powder or metal foil lay-ups between fibres that are compacted and sintered together are a more controllable process. These processes are very labour intensive and costly.
- Also there is the branch introducing the matrix material by deposition processing as physical vapour deposition (PVD) and chemical vapour deposition (CVD).

There are several notable space-based applications of continuously-reinforced MMCs. One major example are structural tubes for the space shuttle orbiters. Each space shuttle orbiter contains 243 MMC tubes in the mid-fuselage main frame and rib truss members, frame stabilizing struts, and in the nose landing gear and drag brace support. The material is 6061 Al with 50% B monofilaments (6061/B/50f), produced by a diffusion-bonded foil-fibre-foil technique. The struts saved 145 kg over the initial design of Al tubes due to the higher specific strength and stiffness of the MMC.

A second example of a continuously-reinforced MMC is the antenna waveguide mast on the Hubble Space Telescope (HST). The mast is made by infiltrating a preform containing carbon fibres with 6061 Al to form a rectangular boom. The Al-MMC antenna waveguide mast does not outgas like many OMC's, thereby avoiding possible contamination of the antenna dish and the optical components of the telescope mirrors. This material also provides excellent oxidation resistance (important for the low earth orbit of the HST). Finally, the antenna waveguide mast is truly multi-functional, providing both structural support for the antenna, and a high-quality electrical path for transmitting radio signals between the spacecraft and the antenna.

Heat Resistance & Radiative Cooling

Materials that can withstand high temperatures are heavily desired for space propulsion. If the combustion chamber or the nozzle can operate at elevated temperatures the requirements for the cooling system are less critical. This usually goes hand in hand with an improvement in performance or reduction of costs. This especially counts for smaller thrusters where the development of a complex regenerative cooling system does not pay off. If such a material can get hot enough so a significant amount of heat flux can be radiated away, radiative cooling takes place. This technique is realised in several space propulsion systems.

The 400 N bipropellant Apogee Motors of Ariane Group are designed to be cooled with two mechanisms. The Thruster is composed out of a platinum alloy that doesn't suffer major loss of mechanical stability even when reaching temperatures of up to 1,800 K. At this temperature the heat flux due to radiation results in a cooling effect. This alone is not sufficient in order to withstand the combustion Temperatures of around 3100 K. The remaining heat is absorbed by a thin film of propellant which is injected onto the walls and vaporizes, namely "film cooling". The downsides of such thrusters are obviously their high density and the excessive use of costly materials.

Carbon reinforced carbon (carbon/carbon) is a long-established material for larger radiation cooled nozzle extensions (e.g. RL-10), heat shields etc. Carbon fibre reinforced silicon carbide (C/SiC) is also used for nozzle extensions and under development as a combustion chamber material. Advantages are the high temperature stability up to 2,000 K, its chemical stability and its low weight. Downsides are an elaborate and costly infiltration process and delamination effects parallel to fibres. The nozzle extension of the merlin vacuum engine is made out of a niobium alloy and also radiatively cooled.

"DragonScale" MMC

Continuous Carbon Fiber Reinforced Metal Matrix Composites unify the best of two worlds. They unite the unique properties of carbon fibers, such as high specific tensile strength and excellent temperature stability with the toughness of a metal. Carbon Fibers keep their excellent mechanical properties at temperatures up to 2,000°C. Together with a metal forming a composite, it results in a much higher strength at elevated temperatures as a part made from pure metal would offer. This is possible because of the reinforcing fibers, which helps sharing the loads that act on the composite. Such reinforcement requires an adequate interface with the metal matrix in order to do so. If properly designed and manufactured, MMCs offer an entirely new solution for high temperature applications.

At TU Wien, a novel manufacturing process for such MMCs is currently under development. This process allows an embedment of carbon fibers into the matrix of different metals. At the moment, the focus of the research lies on the manufacturing of nickel matrix composites. This unique process is performed at lower temperatures and comparably small effort. Furthermore, the flexibility of the process allows the adaption to a variety of applications.

Analysis

A brief approximation for a radiatively cooled nozzle is shown in this section. The thermal transmittance through the walls of a thrust chamber can be described with only few formulas, where following parameters come into play.

Table 47 - DragonScale Properties for Analysis

Parameter	Value
Combustion Temperature, T_c (K)	2,500
Coefficient of Heat Transfer of Combustion Products to Chamber Walls, a ($W/m^2 \cdot K$)	2,000
Thermal Conductivity of Chamber Walls, λ ($W/m \cdot K$)	20
Wall Thickness, δ (mm)	1
Emissivity of Chamber Walls, ε	0.9

The impact of the parameters on the thrust chamber wall shall be approximated. The process is split up in the following steps.

Heat Transfer on the inner combustion chamber wall (factor 1,2 approx. 20% radiation)

$$\dot{q} = \alpha * (T_c - T_{w1}) * 1.2$$

Thermal Conduction of the combustion chamber wall

$$\dot{q} = \frac{\lambda}{\delta} * (T_{w1} - T_{w2})$$

Thermal Radiation from the outer wall

$$\dot{q} = \varepsilon * k * (T_{w2})^4$$

The impact of varying parameters is plotted in below.

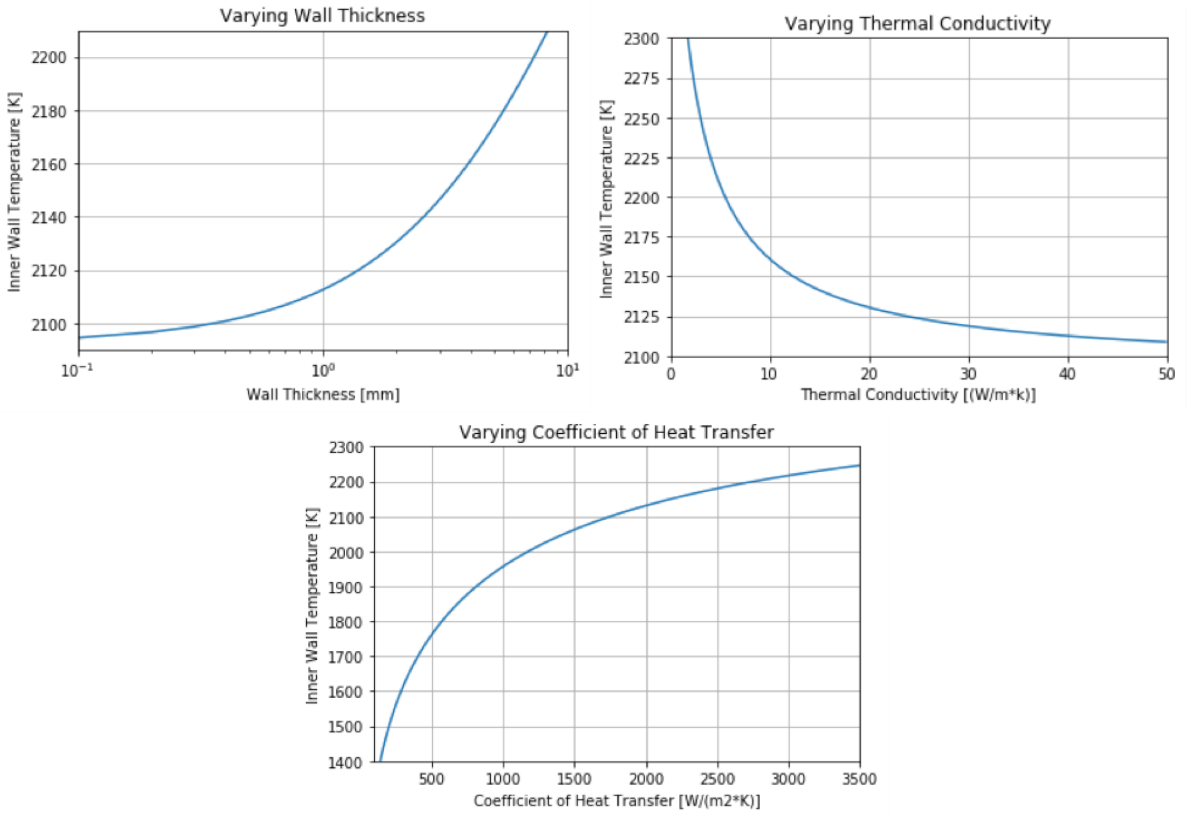

- **Impact of the Thermal Conductivity:**
  The Thermal Conductivity of the material has a minor impact on the inner wall temperature, especially at lower wall thicknesses. If a certain value is reached (approx. 20), no significant temperature decreasing is observed on the inner wall
- **Impact of the Wall Thickness**
  The influence increases with the Wall Thickness, but only slowly. Under 1-2 mm the effect is negligibly small.

- **Impact of the coefficient of Heat Transfer**
  The coefficient of Heat Transfer has the most impact on the system. The reduction of the Heat Transfer will be a major issue.

Calculation of the coefficient of Heat Transfer using Bartz Model.

The Thermodynamic Data from NASA CEA (Chemical Equilibrium with Applications) was used. The temperature of combustion and the gas composition were used to calculate an adiabatic expansion of the gas. The output of the calculation was used to approximate the heat transfer into the combustion chamber and the nozzle using Bartz Equation. The temperatures of the inner wall are plotted according to the Mach Number in the figure below.

The highest heat introduction occurs between Mach Number 0,3-1, meaning the convergent shape of the nozzle. The maximum temperature of the inner wall results in approximately 1950 K in this calculation.

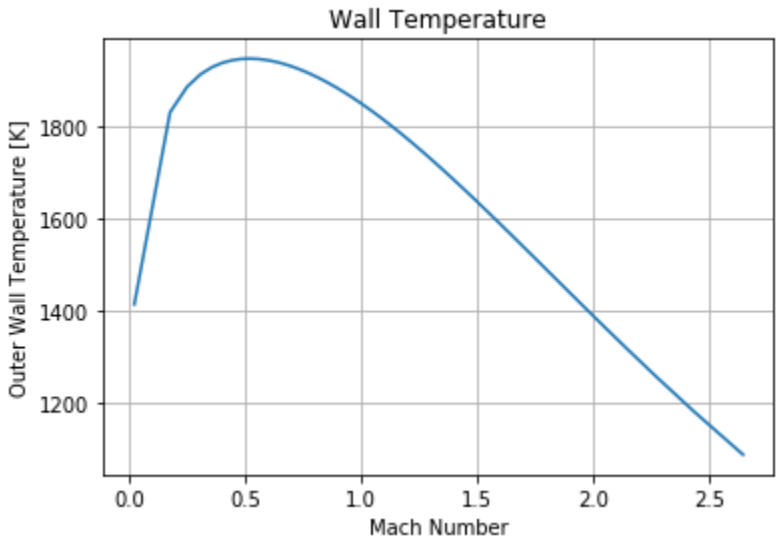

Testing plan

"DragonScale" Manufacturing and Testing

The most important aspects during the development of a composite is related to the interface between the two phases. Only if the connection allows enough interaction to transfer loads, the reinforcement is successful. In the worst case, the properties are affected in a negative way and the pure matrix would offer a better solution. For a proper interface, two things must be optimized:

- **Interface Bonding**: The Bonding shall contain strong molecular interaction between the phases. Real chemical bonds are preferred rather than weak dipole interactions or mechanical friction.
  This can be achieved by surface treatments, coatings or alloying of the matrix
- **Interface Area**: A larger area results in more interaction. Therefore, the matrix shall cover the fibers perfectly, pores and voids need to be minimized.

Using the DragonScale process, it is already shown that the pore volume can be kept very low. A pore volume fraction of less than 10% has been achieved for smaller samples. The optimum parameters for larger samples are still part of the current research. In the figure below, a metallographic cross section is shown. It can be seen how the matrix percolates very well in between the individual carbon fibers.

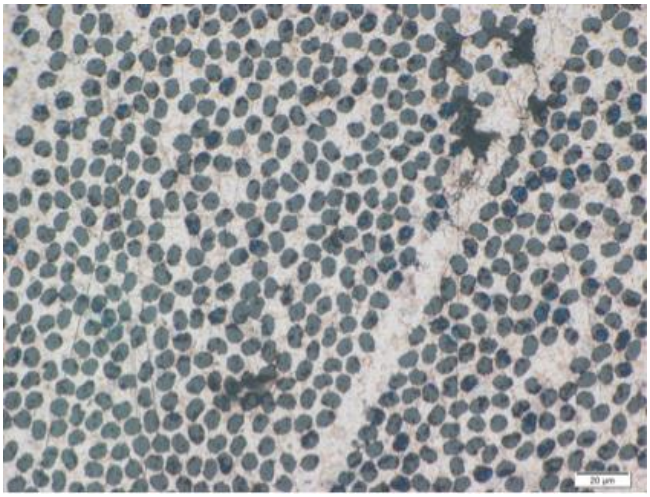

Hydrostatic Pressure Test

The investigation of the interface is slightly more complex because several parameters come into play. There are very elaborate methods to study the interfacial bonding, including single fiber pull-out or push-out tests. Those methods require high precision instruments and careful specimen preparation. For a qualitative analysis which is more in step with the actual praxis, a simpler test was chosen. A hydrostatic pressure test was performed using a specimen of a hollow cylindrical shape. By calculating the loads on the specimen, it is possible to draw back conclusions to the interface of the fiber and the matrix. Furthermore, the investigation of the fracture behaviour can tell a lot about the material.

The specimen for the test had an inner diameter of 20 mm with a wall thickness of about 1 mm. The pressure test was performed until the pressure dropped due to failure of the material. The figure below represents the graph of the testing procedure. The maximum pressure during the test was around 120 bars. The pressure did not drop to zero immediately after the peak, which indicates a gradual failure.

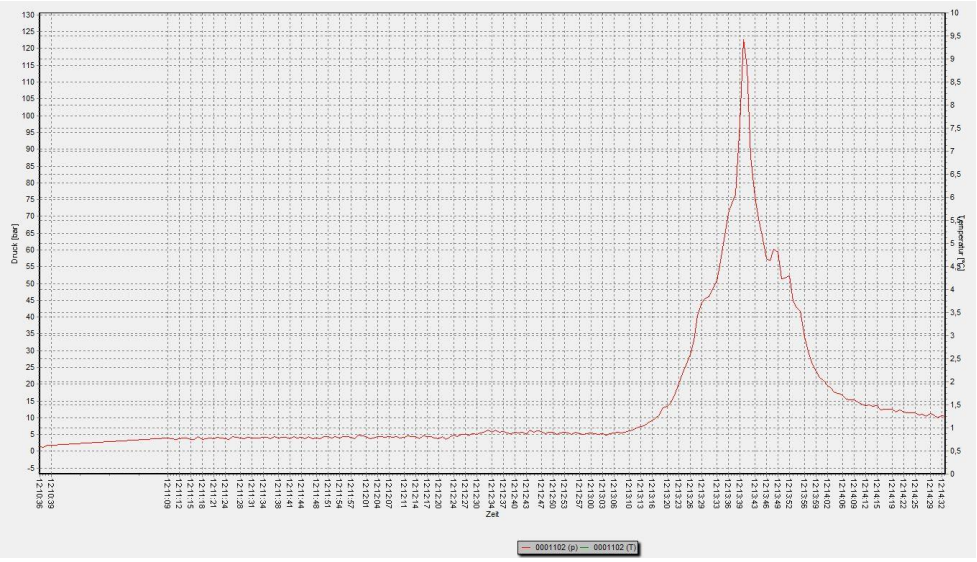

Demonstrative Hot Fire Tests at Schleiffelder Aero

For a proof of concept, the partner company Schleiffelder Aero conducted a hot fire test in early 2018. The small test stand was designed for engine testing up to 300 N. For this purpose, a simple swirl gas-gas injector system was

developed. For the combustion, hydrogen gas was burned with pressurized air. This system ensured a reliable combustion with flexible design. The feed pressures and the mixture ratio could be varied easily and therefore the combustion temperature and chamber pressure was controlled. The DragonScale thrust chamber was mounted on the injector plate and fired without active cooling system. The temperature of the chamber outer wall was approximated through the wavelengths that were emitted. The temperature on the inside was then approximated through with the model from above. A picture of the hot fire test is shown in the figure below

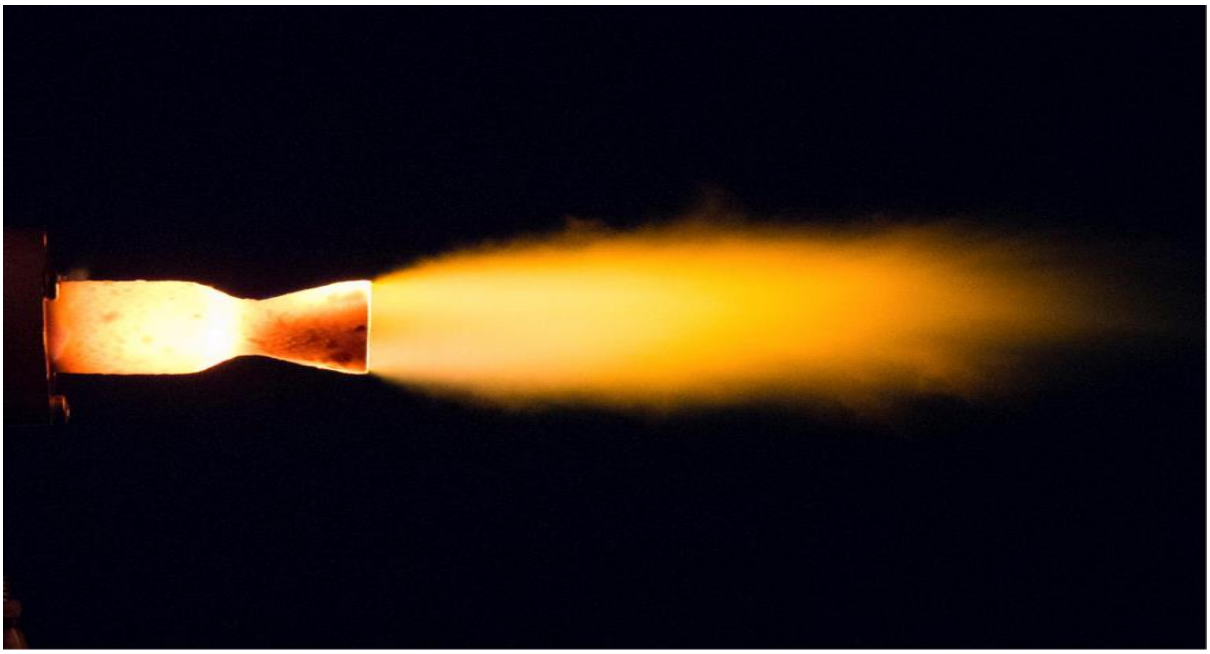

The hottest glowing area of the nozzle clearly is right before the throat section. This matches with the predictions from the approximation with the Bartz equation. The temperature in this section can be easily estimated by comparing the colour of the emitted light.

The hottest area of the nozzle therefore reached a temperature of about 1150 °C on the outer wall and up to 1200 °C in the inner wall. This means the wall temperature exceeded 80% of the melting point (in K) of pure nickel. At this temperature, even the toughest, nickel based superalloys only retain a fraction of their yield strength. The calculated chamber pressure of the test run was around 5 bars. The pure metal would not have been able to withstand the loads at these temperatures, therefore it is a strong indication of a successful reinforcement.

Outlook and Further Testing Plan

For the application on a suborbital rocket there is still lots of development to do. The major tasks involve the upscaling of the process, as well as the improvement of the material using a more capable matrix material.

The upscaling for the Nickel DragonScale has already been tested. Cylindrical components with diameters of 50 mm have successfully been manufactured. The experiments suggest that further upscaling to the size of a full-scale nozzle will be possible.

The substitution of the nickel matrix with metals that are more suitable for the targeted combustion temperatures has been started too. First experiments indicate that the DragonScale process can be applied with chromium. Further research will show the capability of this matrix in the upcoming months. This substitution could lead to a significant improvement of the temperature stability. Assuming that the composite would behave similarly as the nickel matrix type, it would open up further possibilities. If the temperatures stability exceeds 80% of the melting temperature of chromium, we are in temperature ranges where parts of the nozzle and combustion chamber could withstand the

engine operation without any active cooling strategy. This is the goal we are approaching for our thrust chamber material.

Complementary/Alternative Cooling Concepts

Even though the performance of DragonScale has been beyond expectations at all performed tests, it is still in its development phase, therefore the chances, that the material does not live up to expectations, can not be ignored. Loss of combustion chamber integrity due to insufficient thermal or mechanical stability would lead to the necessity of implementing counteracting measures, even up to completely replacing dragon scale with a suitable standard material. In any cases, a suitable alternative/supporting cooling strategy is the key to success. Due to the intentions on using a highest possible ratio of radiative cooling, in combination with the DragonScale high temperature MMC, most cooling mechanisms can be ruled out, due their use requires a specific chamber material (e.g. ablative cooling, transpiration cooling) or prohibit the use of supportive cooling due to its mechanical setup (e.g. regenerative cooling). Out of this reason, the only suitable concept for an alternative cooling system is film cooling. Usually based on two different mechanisms, namely liquid/ evaporation film cooling and gaseous film cooling, this method is used as supportive cooling or as primary cooling method on a variety of Rocket Engines of all sizes. The Amount of Film cooling can be scaled easily without the need of large design changes and is therefore perfectly suitable for hardware based development. However, using a certain portion of propellant for cooling reduces engine performance, therefore the film cooling amount shall be kept to a minimum. During initial Rocket design and especially propellant selection, the risks of using dragon scale were already known, therefore, a fuel with good film cooling characteristics was chosen. Ethanol will therefore be used for film cooling. In the following section, the general principles of film cooling shall be lined out briefly.

Liquid Film Cooling

When using liquid fuel as film coolant, first phase is called liquid film cooling. A certain point of the liquid is injected axially at the combustion chamber wall, mostly by a modified injector. Due to injection speed and gas flow in the chamber (couette flow), this film is transported alongside the combustion chamber wall towards the throat. While travelling downstream, cooling of the chamber walls is provided by three mechanisms. Due to convective heat transfer into the fluid layer, fluid is constantly evaporating at the surface, therefore consuming all the heat induced into the fluid. Furthermore, the gaseous coolant flowing radially inwards is inducing a blowing effect into the boundary layer, therefore reducing heat transfer rate significantly. Thirdly, coolant is evaporated at the wall side due to radiative heating of the combustion chamber wall (most liquids are transparent). The vapor bubbles are also released into the boundary layer, further enhancing the blowing effect. Liquid Coolant Film thickness will continuously decrease due to evaporation and splashing, eventually leading to burnout of the coolant film. The length of the area cooled by liquid film cooling is dependent on combustion chamber geometry (smaller dimensions=more film cooling), coolant mass flow and the type of coolant used.

Gaseous Film Cooling

After liquid film burnout, the cool gases released by evaporating the coolant stays within the boundary layer, creating a “cool” sublayer and thus protecting the engine wall from the hot combustion gases. However travelling downstream, the cold gasses mix with the hot combustion gases, therefore reducing the cooling effect. Turbulence, change of geometry and boundary layer growth increase the mixing effect. Portions of the engine cooled by gaseous film cooling are suspended to significantly higher thermal loads, than those, cooled by liquid film cooling. Gaseous film cooling is often used as support for divergent nozzle extensions. Gaseous film cooling efficiency can be enhanced by reduced turbulence, engine geometry, gas properties and gaseous coolant amount.

By changing the amount of fuel provided for film cooling, the ratio of liquid film cooling to gaseous film cooling can be adapted. While most medium thrust engines rely mostly on liquid film cooling and low temperature materials like stainless steel, Nickel Superalloys (e.g. Armadillo Aerospace), thrusters made of high temperature materials (e.g.

Platinum- Rhodium,...) rely mostly on the gaseous film cooling effect as supportive measures to keep the wall temperature within the capabilities of the material. This technique is mostly used for small scale apogee motors.

Film Cooling Model

As a first estimation for film cooling efforts, a efficient (one dimensional isotropic flow algorithm for variable gas properties developed by TUST is used (about 2 % deviation to NASA CEA) in order to obtain free stream gas and flow conditions over nozzle and combustion chamber. Combustion gas composition and adiabatic flame temperature have been calculated by NASA CEA. For the first estimate, coupling of cooling and free stream gas flow by heat and mass transfer are neglected, detailed coupled calculations will be performed during the upcoming design phase. In order to take combustion into account, a linear rise of temperature between chamber start and half the distance of wall-spray- intersection is used as an approximation. In order to calculate non- film cooling heat transfer coefficients, the localized stanton form of the famous Bartz equation is used.

$$St = \frac{0.026}{Pr^{0.6} Re^{0.2}} \left(\frac{T_e}{T_m}\right)^{0.68} \left(\frac{d^*}{r_c}\right)^{0.1} .$$

Stanton Type Local Bartz Equation

$$\dot{q}_{CO_2} = 4,067 \sqrt[3]{p_{CO_2} L_e} \left(\left(\frac{T_g}{100}\right)^{3.5} - \left(\frac{T_w}{100}\right)^{3.5} \right) , \qquad \left[\frac{W}{m^2}\right]$$

$$\dot{q}_{H_2O} = 4,067 p H_{2O}^{0.8} L_e^{0.6} \left(\left(\frac{T_g}{100}\right)^{3} - \left(\frac{T_w}{100}\right)^{3} \right) . \qquad \left[\frac{W}{m^2}\right]$$

Radiation Model for H2O and CO2

Radiative heat Transfer is calculated for CO2 and H2O. For Liquid Film Cooling, evaporation mass rate is obtained by the means of an energy balance between evaporation energy and convective & radiative heat flux, where for the convective heat transfer, a reduced heat transfer coefficient is used. This reduced heat transfer coefficient represents the reduction in heat transfer due to blowing effects in the boundary layer. By the use of film theory, (Mickley) a simple relation between reduced heat transfer coefficient and mass evaporation rate can be found.

$$\theta = \frac{\phi}{e^{\phi} - 1} \qquad \theta_H = h/h_* \qquad \left(\frac{\Delta_*}{\Delta} \Gamma\right)_H = \frac{\sum_j N_j M_j c_{p_j}}{h_*} \equiv \phi_H$$

Film Cooling Blowing Model as suggested by Mickley

Due this formulation is neglecting the inflation of the boundary layer and therefore the further reduced heat transfer coefficient due to blowing effects, it is considered a conservative upper bound estimation. Creating an implicit equation with mass evaporation rate, for the sake of simplicity, a standard bisection solver is used to solve this system. Fixed Point iteration led to oscillating divergence of the solution at a certain point downstream. Losses due to splashing is taken into account by adding an additional evaporation safety factor. Position of film burnout is determined by subsequently subtracting evaporation rate from initial injected coolant mass flow. After Burnout, the detailed version of gaseous film cooling efficiency algorithm, as presented in (Grissom Film Cooling in Liquid Rocket Engines) is used in order to calculate adiabatic wall temperature alongside the rest of the rocket engine. The calculations have been performed in Python.

Results & Discussion

Calculations regarding film cooling for the proposed Propellant combination and Nozzle geometry have been performed. Assuming the worst case of substituting DragonScale with a standard High Temperature Alloy, sufficient temperature Values can be achieved by introducing 30% Film Cooling (30% of Coolant Mass Flow) at a safety Factor

of 2. This results in full liquid film cooling of the entire combustion chamber, Adiabatic Wall Temperature at the Throat Area is at about 1000 K. Adiabatic Wall Temperatures within the divergent section of the nozzle are significantly higher, however the model is insufficient for obtaining actual wall temperature. Comparing the Temperature curve with lower film cooling rates (20%, 10%) shows a significant improvement. Due to the conservative approach and high introduced safety factors, the film cooling approach is considered feasible as supportive cooling system for the Base11 rocket, although minor changes in rocket performance and layout may be expected.

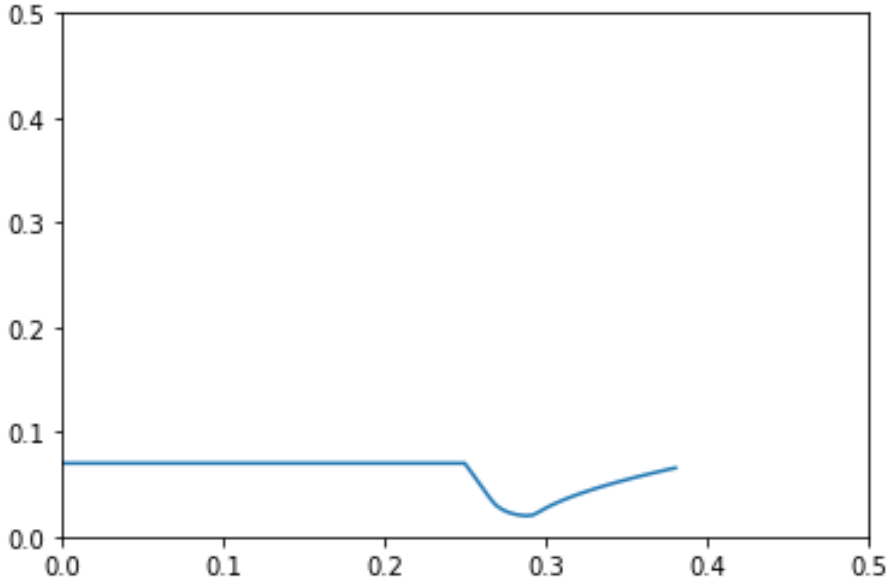

Figure 46 - Nozzle Geometry for film cooling

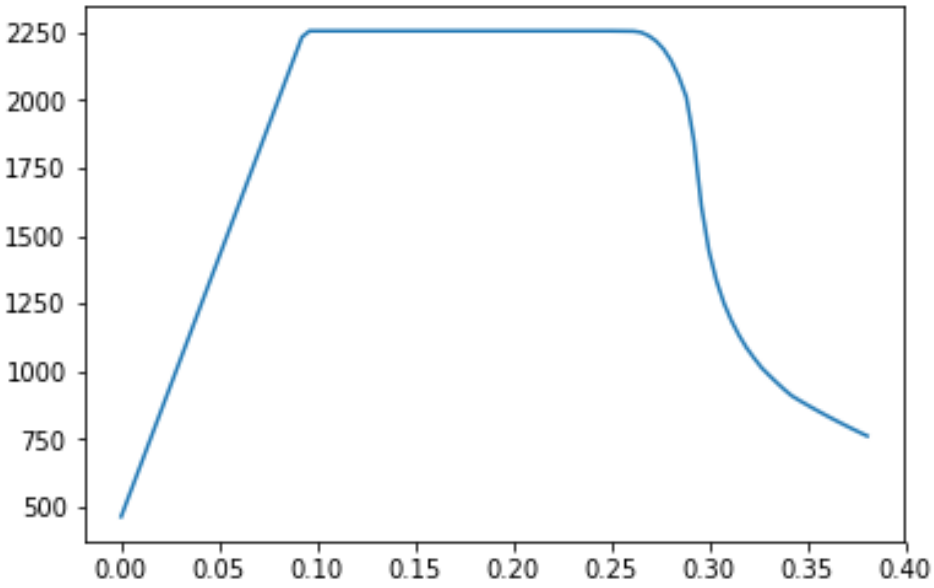

Figure 47 - Free stream temperature profile for film cooling

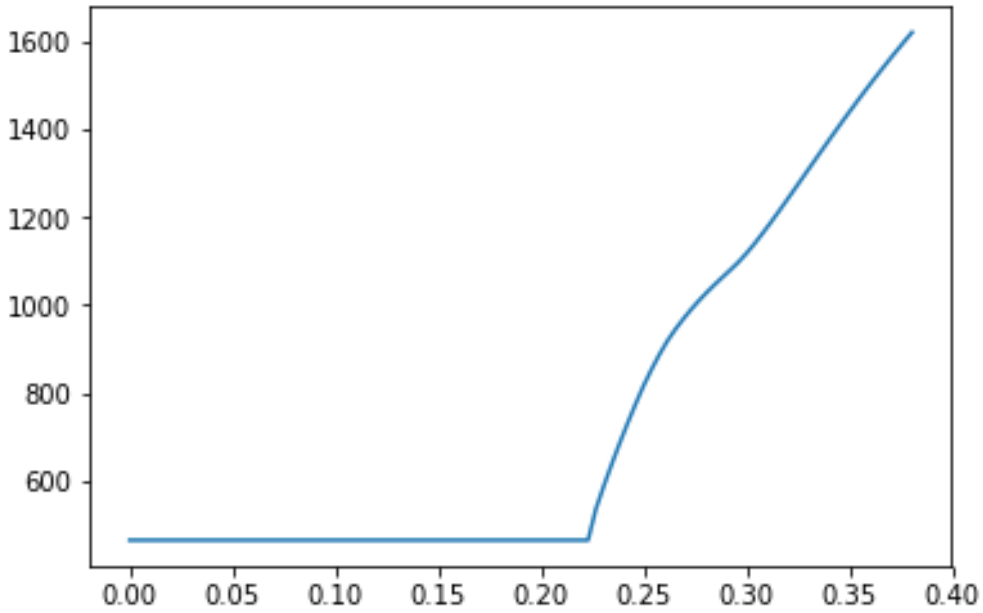

Figure 48 - Adiabatic Wall Temperature for 30% Film Cooling (Safetyfactor = 2)

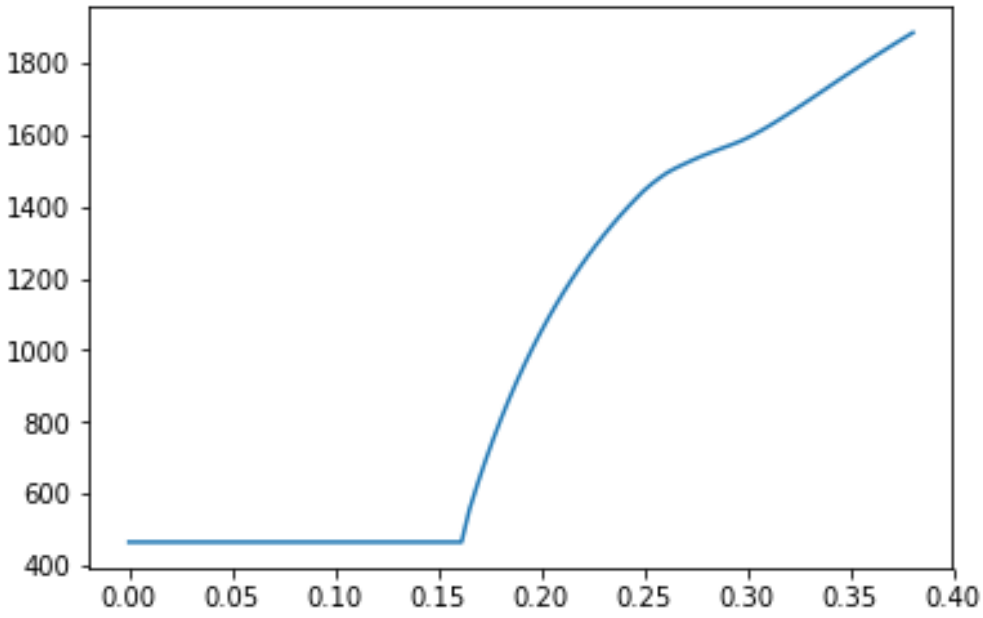

Figure 49 - Adiabatic Wall Temperature for 20% Film Cooling (Safetyfactor = 2)

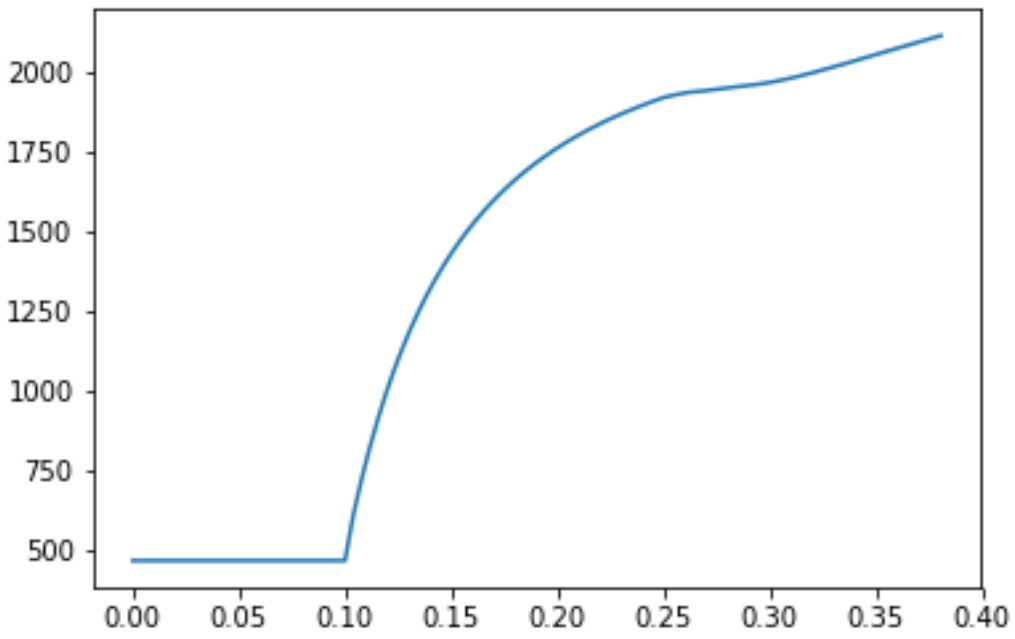

Figure 50 - Adiabatic Wall Temperature for 10% Film Cooling (Safetyfactor = 2)

Experimental Approach & Coolant Injector Design

In order to determine the optimum cooling ratio for the engine, the Engine Test Stand located at Vienna will have a separated coolant tank with autonomous pressure regulation. Designing the cooling injector independent from the fuel injector allows for quick testing of different coolant ratios simply by changing the pressure in the coolant system. Theoretically, different coolant liquids could be tested, however due the Base11 Rocket will be a Bipropellant Rocket, this might not be applicable. ntroducing an electronic pressure control, film cooling rates can be changed during testing, generating the chance of gradually observing the effect of different amounts of coolant. The TUST small scale test stand can potentially updated to monitor interaction between fast gas flow and coolant film within an acrylic chamber. The final injector will be designed in order to be upgradeable to film cooling if required. Fuel and Coolant injection system will be uncoupled, bot systems are fed by separate cavitating venturis connected to the main fuel line, allowing for precise adjusting and quick adaptation of film cooling ratio.

Nozzle

Nozzle Type

This trade study identifies and evaluates the different types of nozzle designs used in rocketry.

Table 48 - Nozzle Design Value Weighting

Criteria	Safety	Simplicity	Cost	Reliability	Performance	Robustness	Score
Safety		1	1	1	1	1	5
Simplicity	0		1	1	1	1	4
Cost	0	0		0	1	1	2
Reliability	0	0	1		1	1	3
Performance	0	0	0	0		1	1
Robustness	0	0	0	0	0		0

Table 49 - Comparison of Nozzle Types

Type	Conical	Bell	Dual Bell	Aerospike	Annular
Performance	Lowest	Medium	High	Highest	Highest
Mass	Medium	Lowest	Medium	High	High
Manufacturability	Simplest	Simple	Medium	Complex	Complex
Heritage	High	High	Low	Very low	Very Low
Design Process	Simplest	Simple	Complex	Complex	Complex
Cost	Lowest	Lowest	Medium	Higher	Higher

Table 50 - Weighted Comparison of Nozzle Types

Criteria	Weight	Conical	Bell	Dual Bell	Aerospike	Annular
Safety	0.33	+	+	+	+	+
Simplicity	0.27	+	+	+	-	-
Cost	0.13	+	+	+	-	-
Reliability	0.20	+	+	+	+	+
Performance	0.07	-	-	+	+	+
Robustness	0	-	-	+	+	+
Total		0.93	0.93	1.00	0.6	0.6

Based on the scores in the above table, the aerospike and annular designs were eliminated. The conical nozzle type was also eliminated as its performance is known to be significantly lower than the bell nozzle types.

Table 51 - Weighted Comparison of Nozzle Type Final Candidates

Criteria	Weight	Bell	Dual Bell
Safety	0.33	+	+
Simplicity	0.27	+	-
Cost	0.13	+	-
Reliability	0.20	+	-
Performance	0.07	-	+
Robustness	0	=	=
Total:		0.93	0.6

From this final comparison, the single bell type was selected for the nozzle geometry. The dual bell nozzle, while having higher performance, is significantly more difficult to design and manufacture. UTAT has developed several in-house codes and simulations for designing and validating single bell nozzles, which provides an advantage in terms of design experience. In terms of manufacturing, the dual bell is sensitive to imperfections that would effectively defeat the advantages over a single bell, while suffering from a mass penalty due to the increased size.

Design

The nozzle contour is a Compressed Truncated Ideal Contour (CTIC), a contouring method developed in-house by UTAT. The contour is generated by first creating a full Ideal contour (IC) using the Method of Characteristics. The ideal contour, in order to isentropically expand the gasses without introducing an internal shockwave, is usually very long and will result in a non-physically feasible design. In practice, whenever an IC is used as a nozzle contour, it is usually truncated and the first 20-60% of the contour is used in the final design, depending on application and constraints. However, in some cases, the contour is still excessively long after truncation, and further truncation

could result in flow separation due to the severe drop in pressure. The following image compares a full ideal contour with a parabolic nozzle that fits the length constraints.

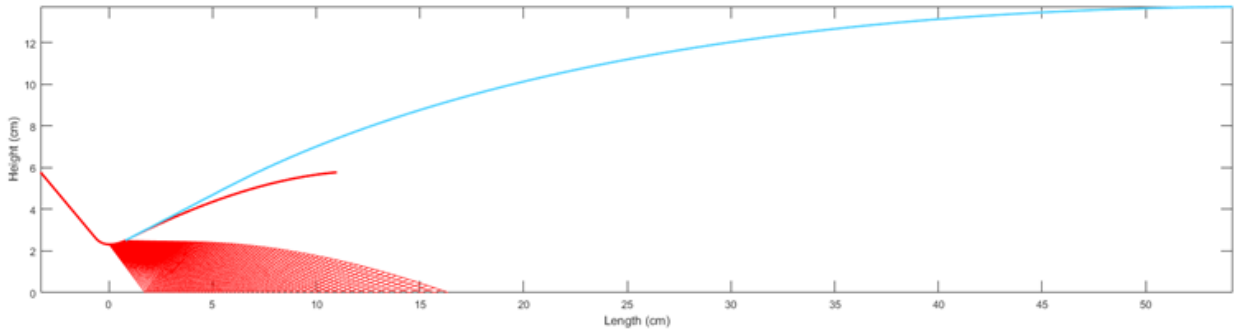

Figure 51 - Comparison of Ideal (blue) & Parabolic (red) Contours

The vast difference in length motivates the development of a method to guarantee shock-free expansion at acceptable nozzle lengths. For the CTIC design, a full ideal contour is generated, truncated to a certain point, and linearly compressed down to fit length requirements. The length requirement comes from the percent bell nozzle concept that originates from the Rao or Parabolic nozzle. Experiments have found that a great balance between efficiency and mass is achieved at around 85% bell length, where further increases in bell length produce highly diminishing returns in efficiency. Thus, the length constraint is set using an 85% bell length, and the truncated nozzle is linearly compressed down until the nozzle length matches this requirement. The design is generated by the UTAT CTIC nozzle contour design code. A screenshot of the user interface is shown below.

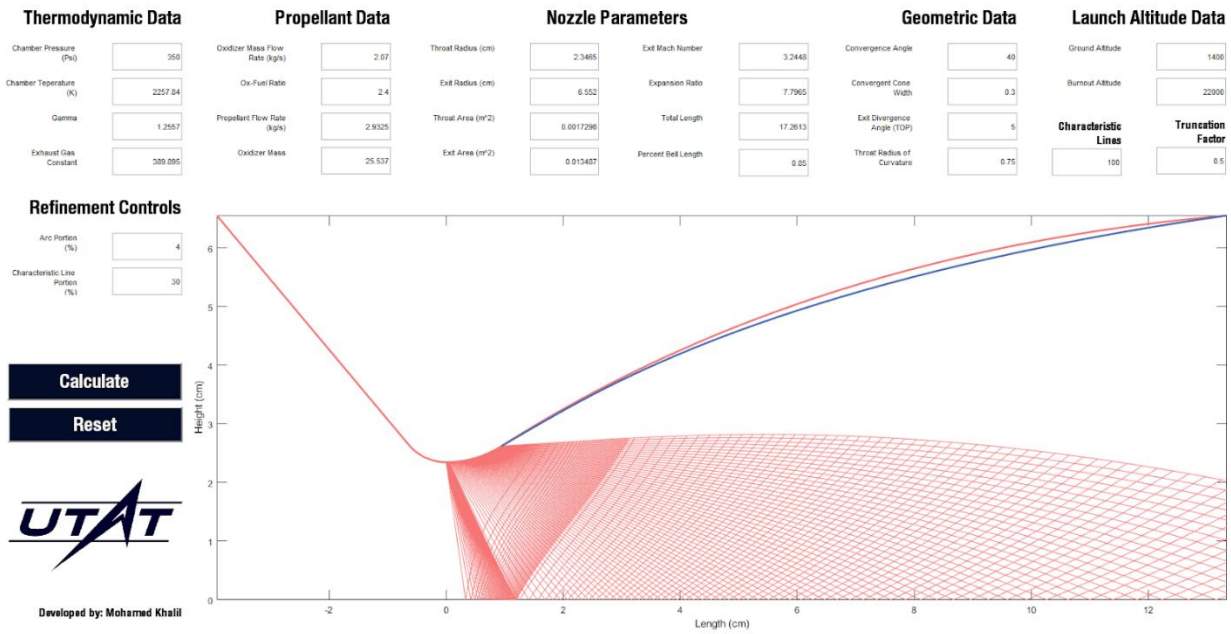

Figure 52 - Screenshot of UTAT Nozzle Design Program Interface

Table 52 - Combustion Chamber Operating Conditions

Property	Value
Chamber Total Temperature (K)	2257.8
Chamber Total Pressure (kPa)	2,416 (350 psi)

Oxidizer Mass Flow Rate (kg/s)	2.07
O/F Ratio, OF	2.4
Specific Gas Constant, R (J/kg·K)	389.95
Ratio of Specific Heats, γ	1.2557

Using the above chamber operating conditions yields a nozzle contour with the following properties.

Table 53 - Nozzle Contour Properties

Property	Value
Length from Throat (m)	0.1334
Expansion Ratio	7.7965
Throat Radius (m)	0.023465
Exit Radius (m)	0.065520
Convergent Section Angle (°)	40

Analysis

The CTIC nozzle has proven, in theory, to eliminate shockwaves in the flow while preventing flow separation. During the earlier development phases of the CTIC design code, CFD analysis was used to track the performance of design iterations. The first iteration starts with no truncation (only compression) and produces an odd-looking nozzle shape. This nozzle shape is not fit for use on the rocket since it produces a strong shock in the flow that is guaranteed to be unstable due to the inherent combustion instabilities (even if minor) in the chamber. The following images show the development of a shockwave inside this contour. Please note that nose nozzles are not the same as the one used on this rocket, they were used in the initial code validation testing phase. It is clear that the final design eliminates the shockwave and produces a more uniform exit velocity profile as compared to the non-optimal solution.

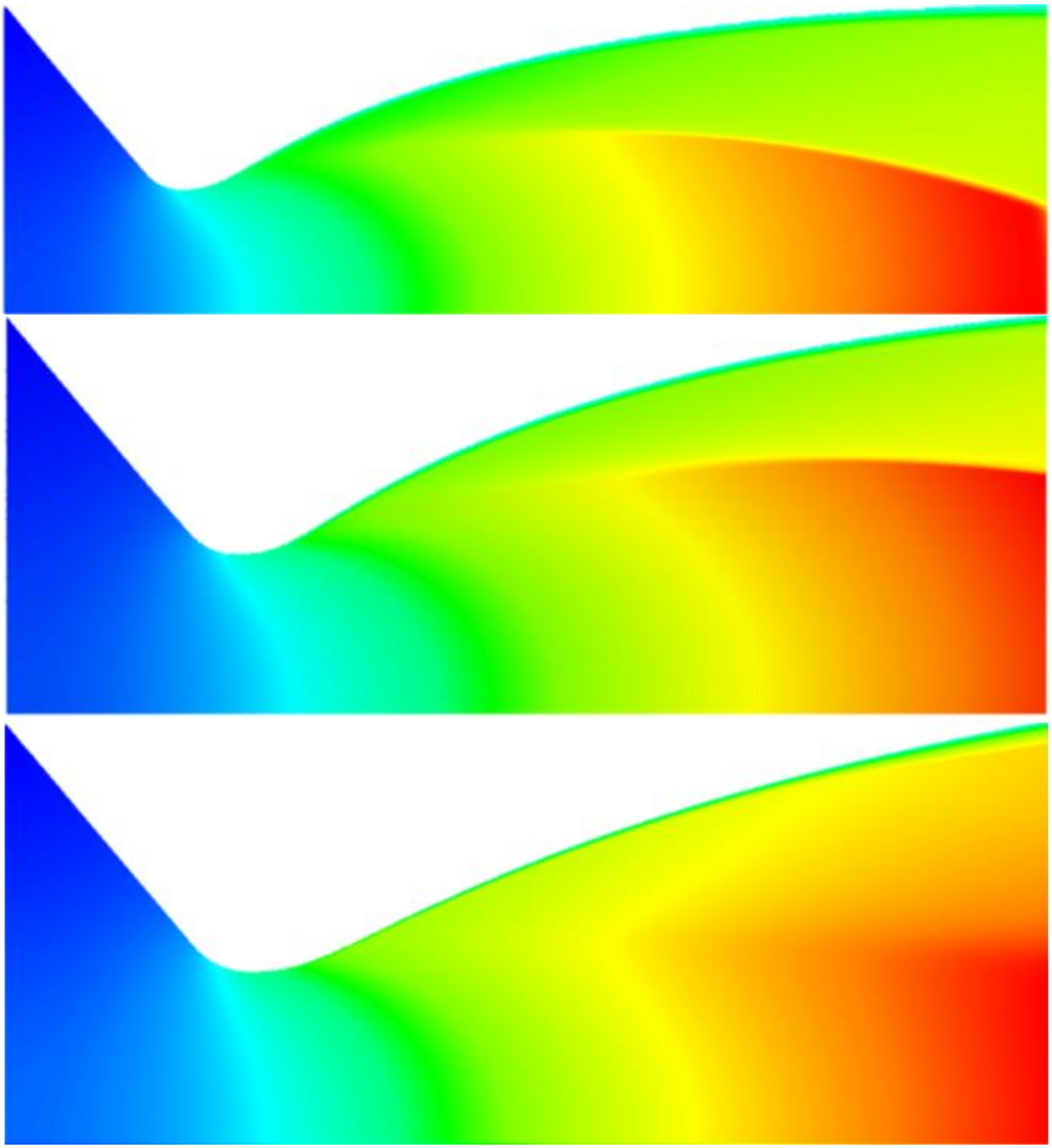

Figure 53 - Internal Shockwave at Varying Truncation Values: 0% (top), 80% (middle), ~45% (bottom)

The CDF will for this nozzle will be performed in the upcoming weeks. The CFD simulation will make use of the following assumptions:

- Frozen flow
- Adiabatic walls
- Uniform inlet velocity
- Ideal gas
- Sutherland Viscosity

- No gravity

The CFD setup is as follows:

- ANSYS 19.1 – FLUENT 2D Transient Axisymmetric Simulation
- Runtime of around XXXXXXXXXXX
- Density Based Solver with Energy Equation coupled
- Standard k-ω turbulence model (Y+ = 1 at wall)
- Tetrahedral Mesh – 508,250 Elements, Bias Factor: 50
- 10 μs time steps

The boundary conditions are as follows:

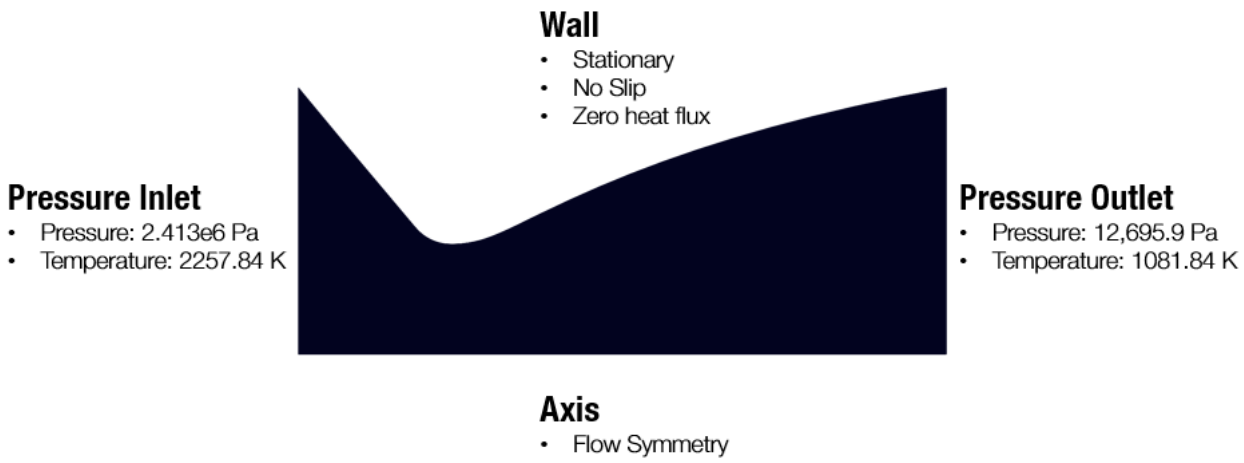

Combustion Modelling and Simulation

The engine simulation script is composed of three main components. The first is a modified MATLAB version of NASA's Chemical Equilibrium with Applications (CEA) code, the next is the NOX blowdown model, and finally, a 2-DOF kinematic altitude model. The CEA component of the script takes oxygen-fuel properties as an input, calculates chemical equilibrium product concentrations (combustion) and outputs theoretical rocket performance by determining the thermodynamic and transport properties for the product mixture. Without any sort of altitude correction, it is difficult to determine the thrust curve of the engine in the preliminary stages of design, therefore the development of an engine simulation provides a more thorough analysis of the engine and subsequently, the performance of the rocket. Below is a flow diagram with a general representation of the engine simulator.

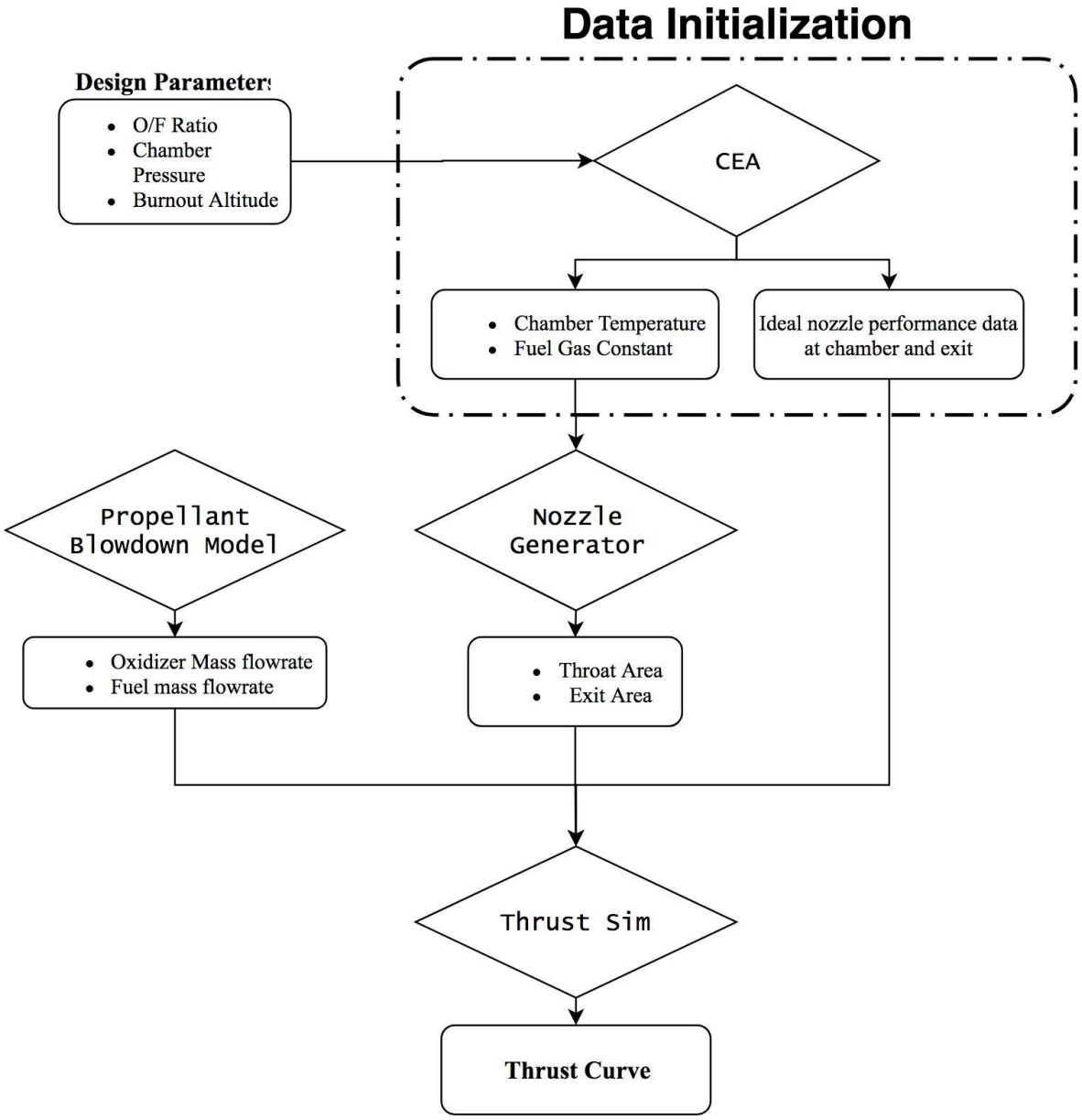

Figure 54 - Combustion simulator flow chart

Code Methodology

The thrust code employs a two-dimensional kinematic model which determines the altitude of the rocket throughout the burn. A flow diagram is provided below illustrating the process and methodology with which the code is written. This section explains the sequence of blocks in the diagram.

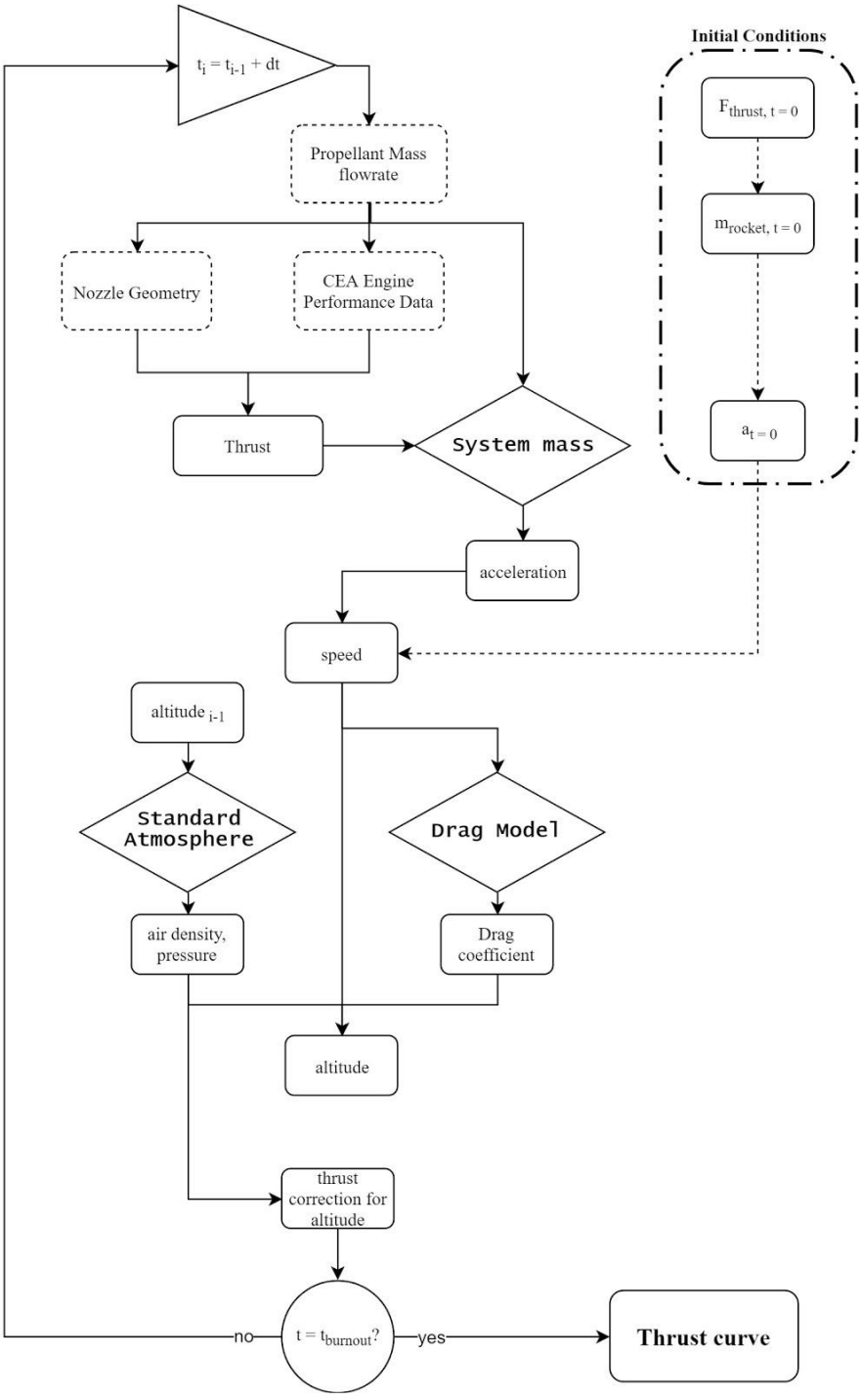

Figure 55 - Combustion simulator code methodology

Item	Description
NASA CEA	Chemical Equilibrium with Applications - A matlab adapted code capable of providing rocket engine performance for various flow properties. This code outputs temperatures, pressures, flow velocities, and etc for the chamber, throat, and exit region of an ideal nozzle.
Nozzle Generator	A function that calculates nozzle geometry from gas dynamics equations for design conditions.
Propellant Blowdown model	A model that outputs the mass flowrate of propellants. (described earlier)
Thrust Simulator	A kinematic based model that can predict the thrust and altitude correction of an engine until burnout.
System Mass	A function that adjusts the mass of the rocket based on propellant flow.
Standard Atmosphere	A model the predicts the air pressure, density, and temperature for a given altitude.
Drag Model	A model that outputs the drag coefficient of the rocket for a given Mach number.

Steps to calculate thrust and thrust correction:

1. Mass flow rate and oxygen-fuel ratio are calculated.
2. Engine performance for oxygen-fuel ratio is determined.
3. Thrust is calculated using engine performance, flow properties, and nozzle geometry
4. Total rocket mass is calculated based on mass flow leaving the rocket.
5. Acceleration of the rocket is determined by equating all the forces acting on the rocket.
6. Kinematic equations are used to calculate speed with a drag model.
7. New altitude is found.
8. Thrust correction is calculated from standard atmospheric properties and iterated.